



**NEAR EAST UNIVERSITY**  
**INSTITUTE OF GRADUATE STUDIES**  
**DEPARTMENT OF BIOMEDICAL ENGINEERING**

**Noise Factor Analysis in Medical Imaging**

**Ph.D. THESIS**

**Omid MIRZAEI**

**Nicosia**  
**January, 2023**

**OMID MIRZAEI**

**Noise Factor Analysis in Medical Imaging**

**Ph.D. THESIS**

**2023**

**NEAR EAST UNIVERSITY  
INSTITUTE OF GRADUATE STUDIES  
DEPARTMENT OF BIOMEDICAL ENGINEERING**

**Noise Factor Analysis in Medical Imaging**

**Ph.D. THESIS**

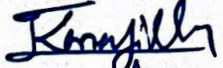
**Omid MIRZAEI**

**Supervisor  
Prof. Dr. Bülent BİLGEHAN**

**Nicosia  
January, 2023**

## Approval

We certify that we have read the thesis submitted by Omid MIRZAEI titled "Noise Factor Analysis in Medical Imaging" and that in our combined opinion it is fully adequate, in scope and in quality, as a thesis for the degree of Doctor of Philosophy in Computer Engineering.

Examining Committee	Name-Surname	Signature
Head of the Committee:	Assoc. Prof. Dr. Tolgay KARANFİLLER	
Committee Member:	Assoc. Prof. Dr. Süleyman AŞIR	
Committee Member:	Asst. Prof. Dr. Payam ZARBAKHSH	
Committee Member:	Asst. Prof. Dr. Ali İŞİN	
Supervisor:	Prof. Dr. Bülent BİLGEHAN	

Approved by the Head of the Department

27/January/2023

  
Assoc. Prof. Dr. Süleyman AŞIR  
Head of the Department

Approved by the Institute of Graduate Studies

/ /2023

  
Prof. Dr. Kemal Hasni Can BAKER  
Head of the Institute  


## **Declaration**

I hereby declare that all information, documents, analysis and results in this thesis have been collected and presented according to the academic rules and ethical guidelines of Institute of Graduate Studies, Near East University. I also declare that as required by these rules and conduct, I have fully cited and referenced information and data that are not original to this study.

Omid MIRZAEI

27/01/2023

## Acknowledgments

I would first like to thank my thesis advisor Prof. Dr. Bülent BİLGEHAN. The door to Prof. Dr. Bülent BİLGEHAN office was always open whenever I ran into a trouble spot or had a question about my research or writing. He consistently allowed this paper to be my own work, but steered me in the right direction whenever he thought I needed it.

I am grateful to my sibling and Parents, my lovely brother Armin and my generous Parents Gholamreza and Shiva.

Foundation for helping and providing the funding for the work. Especially my great thanks for Hüseyin AMCAOĞLU who gave me the opportunity to follow my education with generous fund of TRNC STATE SCHOLARSHIP.

This work would not have been possible without the support of my teachers and my friends Assist. Prof. Dr. Mohammad Momenzadeh, who have been supportive of my career goals and who worked actively to provide me with the protected academic time to pursue those goals.

Thanks for all supports during my studies and efforts to leading to my educational achievement, with all respects to Prof. Dr. Ayşe Gunay Kibarer and Assoc. Prof. Dr. Süleyman AŞIR.

And finally, last but by no means least, also to all my lecturers and friends who supported me in this island specially Prof. Dr. Kaya SÜER Assoc. Prof. Dr. Aslı AYKAÇ, Şerife KABA, and Ahmet ILHAN who helped me to achieve the procedure of my thesis.

**Abstract****Noise Factor Analysis in Medical Imaging****Mirzaei, Omid****Ph.D., Department of Biomedical Engineering****January, 2023, 62 pages**

The statistical properties in various medical images demonstrate uncorrelated noise fluctuations. The signal noise fluctuations are generally due to physical imaging processes and have nothing to do with the tissue textures. Adding the noise types (e.g., quantization, electronics, photon) usually degrade medical images. The noise variation is usually assumed to be additive with zero-mean, constant variance Gaussian distribution. However, close consideration of different medical images indicates the need for better model representation to minimize the noise that can be vital in decision-making. This research proposed a probabilistic method to represent all real-type noise in general medical images. The method aims to cover most classical statistical models such as Gaussian, lognormal, Rayleigh, Weibull, and Nakagami without a prior examination to test for fitness. The proposed model was applied to actual clinical images to test the performance of the noise originating from the physical processes. The noise is assumed to be additive white Gaussian type with a zero mean and constant variance. The theoretical literature indicates that a non-linear function can better represent noise. This research helps to form a relationship between the image intensity and the noise variance that yields the fitting parameters in the introduced nonlinear function. The validity of the proposed method was proved mathematically and tested using the well known Kolmogorov–Smirnov (K-S) and Akaike Information Criteria (AIC) tests. The method was successfully applied to various clinical images such as magnetic resonance, x-ray, and panoramic images. The model's performance is compared with the classical models using root mean squared error (RMSE), relative error (RE), and  $R^2$  as the evaluation matrices. The presented model has outperformed all classic models.

**Keywords:** image noise, medical image, noise distribution, probabilistic noise model, statistical noise

## Özet

### Tıbbi Görüntülerde Gürültü Analizi İçin Güçlü Bir Olasılık Modeli

Mirzai, Omid

Doktora, Biyomedikal Mühendisliği Bölümü

Ocak, 2023, 62 sayfa

Çeşitli tıbbi görüntülerdeki istatistiksel özellikler, ilişkisiz gürültü dalgalanmalarını gösterir. Sinyal gürültü dalgalanmaları genellikle fiziksel görüntüleme işlemlerinden kaynaklanır ve doku dokularıyla hiçbir ilgisi yoktur. Gürültü türlerinin eklenmesi (ör. kuantizasyon, elektronik, foton) genellikle tıbbi görüntülerin kalitesini düşürür. Gürültü değişiminin genellikle sıfır ortalamalı, sabit varyanslı Gauss dağılımı ile toplamsal olduğu varsayılır. Bununla birlikte, farklı tıbbi görüntülerin yakından incelenmesi, karar vermede hayati öneme sahip olabilecek gürültüyü en aza indirmek için daha iyi model sunumuna ihtiyaç duyulduğunu gösterir. Bu araştırma, genel tıbbi görüntülerdeki tüm gerçek tip gürültüleri temsil etmek için olasılıksal bir yöntem önermiştir. Yöntem, önceden uygunluğu test etmek için bir inceleme yapmadan Gaussian, lognormal, Rayleigh, Weibull ve Nakagami gibi klasik istatistiksel modellerin çoğunu kapsamayı amaçlar. Önerilen model, fiziksel süreçlerden kaynaklanan gürültünün performansını test etmek için gerçek klinik görüntülere uygulandı. Gürültünün, sıfır ortalamalı ve sabit varyanslı toplamsal beyaz Gauss tipi olduğu varsayılır. Teorik literatür, doğrusal olmayan bir fonksiyonun gürültüyü daha iyi temsil edebileceğini göstermektedir. Bu araştırma, tanıtılan doğrusal olmayan fonksiyonda uydurma parametrelerini veren görüntü yoğunluğu ile gürültü varyansı arasında bir ilişki oluşturmaya yardımcı olur. Önerilen yöntemin geçerliliği matematiksel olarak kanıtlanmış ve iyi bilinen Kolmogorov-Smirnov (K-S) ve Akaike Bilgi Kriterleri (AIC) testleri kullanılarak test edilmiştir. Yöntem, manyetik rezonans, röntgen ve panoramik görüntüler gibi çeşitli klinik görüntülere başarıyla uygulandı. Modelin performansı, değerlendirme matrisleri olarak ortalama hatanın karesi (RMSE), bağıl hata (RE) ve R<sup>2</sup> kullanılarak klasik modellerle karşılaştırılır. Sunulan model, tüm klasik modellerden daha iyi performans gösterdi.

**Anahtar Kelimeler:** görüntü paraziti, tıbbi görüntü, gürültü dağılımı, olasılıksal gürültü modeli, istatistiksel gürültü

## Table of Contents

Approval.....	i
Declaration .....	ii
Acknowledgments .....	iii
Abstract .....	iv
Özet .....	v
Table of Contents .....	vi
List of Tables.....	viii
List of Figures .....	ix
List of Abbreviations.....	xi

### CHAPTER I

Introduction.....	1
Preliminary .....	1
Noise in Biomedical Image processing .....	1
Some definition and concept in probability .....	4
Maximum Likelihood Estimation (MLE) .....	13
Noise Extraction Methods, Medical Image Filtering .....	16

### CHAPTER II

Literature Review.....	23
Related Works.....	23

### CHAPTER III

Methodology .....	27
Proposed Probabilistic Methodology .....	27
Moment Properties .....	29
The adopted test procedure .....	34

### CHAPTER IV

Results .....	37
Validation procedure for the best-fitting model.....	51

## CHAPTER V

Conclusion .....	53
REFERENCES.....	54
APPENDICES .....	55
Appendix A: Ethical Approval Document.....	59
Appendix B: Curriculum Vitae .....	60
Appendix C: Similarity Report .....	62

## List of Tables

<b>Table 1.</b> Median $E(X)$ , $E(X^2)$ and $\text{Var}(X)$ of Random Variable $X$ for Some Values of $\alpha$ , $\beta$ and $q$ . .....	31
<b>Table 2.</b> Comparison Results.....	38
<b>Table 3.</b> The Goodness-of-Fit Test Results of The Oral Panoramic Radiograph Image.....	41
<b>Table 4.</b> The Goodness-of-Fit Test Results of The MR Image of Human Brain .....	44
<b>Table 5.</b> The Goodness-of-Fit Test Results of The MR Shoulder Image.....	46
<b>Table 6.</b> The Goodness-of-Fit Test Results of The Pathological Shoulder MRI Image .....	48
<b>Table 7.</b> The Goodness-of-Fit Test Results of The Abdominal CT Image .....	50
<b>Table 8.</b> Fitness Verification for The Distribution Models of The MR Shoulder Image.....	51
<b>Table 9.</b> Fitness Verification for The Distribution Models of The Oral Panoramic Radiograph Image .....	52

## List of Figures

<b>Figure 1.</b> Effect of noise in signal .....	2
<b>Figure 2.</b> Diagram of Continuous distribution function .....	6
<b>Figure 3.</b> The Gaussian distribution function with different standard deviations .....	9
<b>Figure 4.</b> Windows and gray -level modification .....	10
<b>Figure 5.</b> Rayleigh distribution with different standard deviations.....	11
<b>Figure 6.</b> Poisson distribution with different lambda .....	12
<b>Figure 7.</b> The dot plot diagram of 10 observations .....	14
<b>Figure 8.</b> The data points and possible Gaussian distributions .....	15
<b>Figure 9.</b> Median Filter for The Array of Observations .....	17
<b>Figure 10.</b> Median Filter for The Matrices of Observations .....	18
<b>Figure 11.</b> Mean Filter for The Matrices of Observation .....	19
<b>Figure 12.</b> Effect Of Median Filter in Given Image .....	19
<b>Figure 13.</b> Effect Of Mean Filter in Given Image .....	19
<b>Figure 14.</b> Characteristic Plots .....	31
<b>Figure 15.</b> Flowchart Representation .....	36
<b>Figure 16.</b> Oral panoramic radiograph image .....	39
<b>Figure 17.</b> Histogram of the random noise in OPG .....	40
<b>Figure 18.</b> comparison of the distribution plots of the OPG image .....	40
<b>Figure 19.</b> MR image of human brain .....	42
<b>Figure 20.</b> Histogram of the random noise in MR image of human brain .....	42
<b>Figure 21.</b> Comparison of the distribution plots of the MR image of human brain. ....	43
<b>Figure 22.</b> MR healthy shoulder image.....	44
<b>Figure 23.</b> Histogram of the random noise in MR healthy shoulder image .....	45
<b>Figure 24.</b> Comparison of the distribution plots of the MR healthy shoulder image.....	45
<b>Figure 25.</b> Pathological shoulder MRI image .....	46
<b>Figure 26.</b> Histogram of the random noise Pathological shoulder MRI image .....	47
<b>Figure 27.</b> Comparison of the distribution plots of the Pathological shoulder MRI image.....	47
<b>Figure 28.</b> Abdominal CT image .....	49
<b>Figure 29.</b> Histogram of the random noise abdominal CT image .....	49

**Figure 30.** Comparison of the distribution plots of the abdominal CT image ..... 50

## List of Abbreviations

<b>MRI:</b>	Magnetic Resonance Imaging
<b>CT:</b>	Computed Tomography
<b>US:</b>	Ultrasound
<b>PDF:</b>	Probability Distribution Function
<b>PMF:</b>	Probability Mass Function
<b>CDF:</b>	Cumulative Distribution Function
<b>MLE:</b>	Maximum Likelihood Estimation
<b>MSE:</b>	Mean Square Error
<b>RMSE:</b>	Root Mean Square Error
<b>PSNR:</b>	Peak signal-to-noise ratio
<b>SNR:</b>	signal-to-noise ratio
<b>SF:</b>	Smoothing Filter
<b>MF:</b>	Median Filter
<b>MPF:</b>	Midpoint Filter
<b>HFM:</b>	Hybrid Filtering Method
<b>K-S:</b>	Kolmogorov-Smirnov
<b>AIC:</b>	Akaike Information Criteria
<b>ML:</b>	Maximum Likelihood
<b>NLME:</b>	Nonlocal Maximum Likelihood Estimation
<b>NLML:</b>	Nonlocal Maximum Likelihood
<b>MAP:</b>	Maximum a- Posterior
<b>RE:</b>	Relative Error
<b>R<sup>2</sup></b>	R-Squared Error

## CHAPTER I

### Introduction

In this chapter, some concepts and definitions are introduced that support our work through this dissertation. These discussions cover a wide range of definitions, from medical imaging to some probability concepts.

#### Preliminary

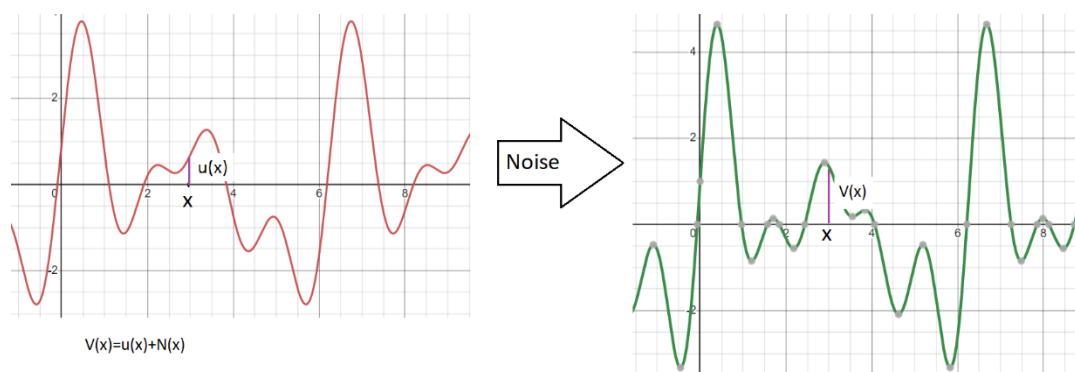
In order to diagnose, monitor, or treat medical disorders, the term "medical imaging" refers to a number of different technologies that are used to view the human body. Each technology type provides distinct information regarding the part of the body being investigated or treated in relation to potential disease, injury, or the efficacy of medical treatment. These medical technologies such as Magnetic resonance imaging (MRI), Computed tomography (CT), Xray, Ultrasound and etc. are increasingly used by the medical community for the diagnosis, staging, and treatment of many diseases as a result of the intrinsic advancement in low-cost imaging and computational technologies. In addition to being a prospective subject for atomic physics study, the field of medical imaging is quickly becoming a vital diagnostic tool in both conventional and cutting-edge hospitals around the globe (Zhou et al., 2021; Chen et al., 2022).

In order to better diagnose any pathological symptoms, medical images must be free of any artifacts and noises that do not cause serious consequences to the patient. One of the most important factors in the field of medical image processing is to reduce artifacts and noise as much as possible without damaging the main information of the image.

#### Noise in biomedical image processing

In this section, some definitions are introduced about the noises that can be seen in the medical area. Noise in biomedical signals: Any unwanted signal that tampers with the signal of interest is considered biomedical noise. Indeed, the noise is an unwanted interruption in the original data, and this can be seen in any modification to the original image or signal (Ferdjallah & Barr, 1994). For instance, consider the following figure that determines the effect of noise in the original signal:

Figure 1.

*Effect of noise in signals*

As it can be seen in the above figure, the original signal can be expressed as a function of  $x$ , where  $x$  denotes the location on the horizontal axis. By implementing the noise on this signal, the result will be another signal where any value can again be expressed in terms of  $x$ . Here,  $V(x)$  denotes the value of the signal at  $x$ , after which the noise is applied. Therefore, the modified signal  $V(x)$  can be written as the original value  $u(x)$  plus the effect of noise at  $X$  or  $N(x)$  (Sundararaj, 2019).

Noise comes from a variety of sources. Some of the sources of noise are heat produced by the electronics, static electrical signals in the surroundings, and movement between the subject and the sensors (Kher, 2019).

Noise in medical imaging Undesired information that taints the image is referred to as noise. Noise is an important factor that degrades the quality of medical images and is known as the random change in the optical density of the image (Mohd Sagheer & George, 2020; Prabu et al., 2019). The most significant impact of noise in medical imaging is the determination of observed object boundaries. This may make diagnostic characterization or object size more challenging (Karimi et al., 2020).

In addition, these images are grayscale, and the effect of the noise can be seen as a modification in the gray level. In other words, the noise can affect the image by interfering with the gray level of some pixels, and as a result, a blurred image can be seen. The gray level of the image is categorized and scaled with a real number in the interval  $[0, 255]$ . This number indicates the brightness of the specific pixel. The minimum gray level is 0, and the maximum gray level depends on the digitalization depth of the image. For an 8-bit-deep image, it is 255. In a binary image, a pixel can

only take on either the value 0 or the value 255. By this explanation, the noise can be seen as a modification of the original image's colors (gray level) in the blur image (Nitta et al., 2019).

The smoother the image, the less noise there is (Mohd Sagheer & George, 2020). Information on the type of noise present in the original image is crucial during the denoising process. The nature of the noise can be expressed with different methods. The statistics tools may can be considered to determine the noise. In this case, the noise can be characterized by the probability distribution related to the defined random variable. These concepts briefly introduced in the next section.

Medical diagnosis accuracy can be affected by noise in medical images, and as a consequence the diagnostic value of the imaging modality is questioned. It was mentioned before that the noise can be expressed by probability distribution function. Thus, the different medical imaging devices with their related noise distribution can be listed as follows:

- 1) X-Ray: Gaussian and Poisson (Kiran et al., 2019; Göreke, 2023)
- 2) CT: Gaussian, Quantum noise (Heylen et al., 2022; Zhang & Wang, 2022)
- 3) Positron emission tomography (PET): Gaussian (Yu & Muhammed, 2016)
- 4) single-photon emission computerized tomography (SPECT): Gaussian (Nikolov et al., 2022)
- 5) MRI: Gaussian, Rician, Rayleigh (Elaiyaraja et al., 2019; Pankaj et al., 2021; Zhang et al., 2022)
- 6) US: Gaussian, Sound waves (Wang et al., 2022; Guan et al., 2021)

The technique used to remove the noise from the image depends on the type of image and the noise model. Several techniques exist to filter noise without impairing crucial aspects of images (Pal et al., 2017).

## Some definitions and concepts in probability

In this section, some definitions and concepts are introduced about probability and statistics. The onset of the probability concept can be traced back to gambling games. Every day, people face unexpected events with uncertain results. Here, the main deal and purpose is statistical experiments with many possible outputs. If the collect of all possible outcomes of a single statistical experiment into a set is considered, then the resulting set is called sample space. If the noise is interpreted as a change in the gray level of all pixels in an image, then the sample space is all pixels in the original image. An event is defined as a subset of sample space. In this way, the events are a set of sample points that involve some specific happenings.

When there is a discussion about the probability, our purpose is the probability of an event. The probability system is an axiomatic system that assigns a numerical value to each event. The probability of an event is a real number between zero and one that determines its possibility of occurring. Certain events have a probability of 1, and impossible events have a probability of zero. There are three axioms in probability that are listed here:

- 1) The probability of the sample space should be equal to one.
- 2) The probability of an event is a numerical value between zero and one.
- 3) If  $A_1, A_2, \dots, A_n$  are mutually exclusive events (i. e.  $A_i \cap A_j = \emptyset$  for  $i \neq j$ ) then

$$P(\cup A_i) = \sum_{i=1}^n P(A_i).$$

With the aid of these axioms, It can be seen that the probability of an event, if all sample points have the same chance of occurring, is equal to the cardinality of the event over the cardinality of the sample points. The cardinality of the set is simply defined as the number of elements in that set. Therefore, the probability of getting heads in the experiment of tossing a coin is equal to half if the coin is unbiased.

In addition, the definition of conditional probability arises from considering the happening of an event in relation to another event. To illustrate the situation, one may consider the probability of bringing an umbrella. This event is contingent on the outcome of other events. For instance, if the forecast indicates a rainy day, then the probability of bringing an umbrella is increased. The conditional probability can be defined as follows: the expression on the left is read as “the probability of A given B”.

$$P(A|B) = \frac{P(A \cap B)}{P(B)}, \quad P(B) \neq 0$$

The multiplicative rule will result if both sides of the conditional probability are multiplied by  $P(B)$ . Roughly speaking, two events are independent if the occurrence of one does not affect the occurrence of another. In other words, two events are independent if the following condition is satisfied:

$$P(A|B) = P(A) \text{ \& } P(B|A) = P(B) \rightarrow P(A \cap B) = P(A) \cdot P(B)$$

This condition can be generalized to many events. i.e., the events  $A_1, A_2, \dots, A_n$  are independent if and only if  $P(\cap_{i=1}^n A_i) = \prod_{i=1}^n P(A_i)$ .

Furthermore, numerical value can be assigned to each element of sample space (sample points). This corresponding mapping is called the random variable. Two types of random variables can be considered. 1) discrete: If sample points are countable or finite, then the corresponding random variable is discrete. In this case, the gap between the sample points can be found. 2) continuous: If the sample space is homomorphic with the real-valued interval and the sample points are uncountable, then the random variable is continuous.

For example, in the coin toss experiment, the sample space contains two elements, or sample points, and  $S = \{Head, tail\}$ . In this case, the corresponding random variable is discrete, and any two numbers can be assigned to express the sample points. As an example of a continuous random variable, consider the experiment in which a computer selects a random real number through the interval  $[0, 1]$ . Now the sample space contains all real numbers in that interval, which is uncountable. It is obvious that there is no bijection between the integers and all real numbers in  $[0, 1]$ . In this case, the random variable can be defined as a value that has occurred.

Another related topic is the probability distribution function (PDF) or probability mass function (PMF). Here, the probability of each sample point is plugged. The PDF determines how the probability is distributed for each sample point. In the discrete case, the PDF is a function, let say  $f_X(x)$  with the following properties:

- 1)  $f_X(x_i) = P(X = x_i)$
- 2)  $0 \leq f_X(x) \leq 1$
- 3)  $\sum_x f_X(x) = 1$

The variance of a given random variable can be defined as an average of  $(x_i - \mu_X)^2$ . Thus,

$$\text{Var}(X) = \sigma_X^2 = \sum (x_i - \mu_X)^2 \cdot f_X(x_i)$$

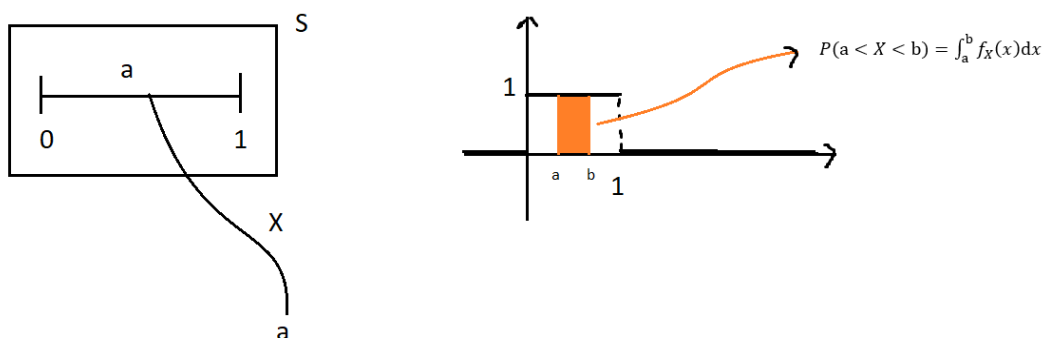
This measurement determines the average of the squared deviations of a random variable. Here, the expected value is subtracted from each value of the random variable and then square it and multiply it by the corresponding probability. Similarly, the PDF of the continuous random variable can be defined as well. Here, it is important to care about the probability of one specific value. Due to the size of the sample space, which is even uncountable, the probability of one specific value being chosen will be zero. Therefore, for a continuous random variable, PDF cannot represent the probability of that sample point, and instead, the probability of one interval has a meaning. The PDF of a continuous random variable has the following properties:

- 1)  $P(a < X < b) = \int_a^b f_X(x) dx$
- 2)  $0 \leq f_X(x) \leq 1$
- 3)  $\int_{-\infty}^{\infty} f_X(x) dx = 1$

Now, let us consider the previous example of a continuous random variable. In that statistical experiment, a random number would be selected from the interval  $[0, 1]$ . Let  $X$  represent the number that occurred, and all numbers in the given interval have the same chance of occurring. As a result, the distribution function will be uniform, and the probability of each sample point will be equal. Since the integral of PDF over the real line should be equal to one, the given PDF should be equal to 0.5 in the interval  $[0, 1]$  and zero elsewhere. It is notable that the integral expresses the area under the curve in the given region. The following figure determines the situation:

Figure 2.

*Diagram of Continuous distribution function*



Can define the expected value and variance of this random variable with the aid of integration instead of summation. The result will be

$$E(x) = \mu_X = \int_{-\infty}^{\infty} x f_X(x) dx$$

$$Var(X) = \sigma_X^2 = E(x - \mu_X)^2 = \int_{-\infty}^{\infty} (x - \mu_X)^2 f_X(x) dx$$

The cumulative probability of any given function below, above, or between two points is expressed by a cumulative distribution function (CDF). The CDF tracks the cumulative probabilities up to a specific threshold, much like a frequency table counts the total frequency of an occurrence up to a certain value. The cumulative distribution function is denoted by  $F_X(x)$ , and the related function for discrete and continuous random variables is defined as

$$F_X(x) = P(X \leq x) = \sum_{x_i \leq x} f_X(x_i)$$

$$F_X(x) = P(X \leq x) = \int_{-\infty}^x f_X(t) dt$$

The idea of a probability distribution function can be generalized to higher dimensions. Indeed, a function can be considered a machine, rule, or mapping of some inputs to some outputs, and the PDF is not an exemption. Most uncertain happenings in real life can be expressed by more than one random variable. Therefore, the input of the PFD can be expressed as an ordered pair of real numbers, and the given function in this case is called the joint probability distribution.

Therefore, the joint probability distribution function of two continuous random variables can be expressed as a function  $z = f_{X,Y}(x, y)$  with the shape of a surface. This function satisfies the following properties:

- 1)  $P((x, y) \in R) = \iint_R f_{X,Y}(x, y) dA$ , *R is a region in  $\mathbb{R}^2$*
- 2)  $\int_{-\infty}^{\infty} \int_{-\infty}^{\infty} f_{X,Y}(x, y) dA = 1$
- 3)  $f_{X,Y}(x, y) \geq 0$

Note that, due to the nature of a continuous random variable, the probability of one specific point in 2-dimensional space should be equal to zero. Here, it is possible to discuss the probability of one region (instead of an interval in one

dimension). Similarly, the expected value of X and Y, can be defined respectively, as follows:

$$E(X) = \int_{-\infty}^{\infty} \int_{-\infty}^{\infty} x \cdot f_{X,Y}(x, y) dA, \quad E(Y) = \int_{-\infty}^{\infty} \int_{-\infty}^{\infty} y \cdot f_{X,Y}(x, y) dA,$$

Since the variance can be interpreted as an average of the squared deviation of a random variable from the mean, the variance of X is defined as

$$Var(X) = \sigma_X^2 = E(X - \mu_X)^2 = \int_{-\infty}^{\infty} \int_{-\infty}^{\infty} (x - \mu_X)^2 \cdot f_{X,Y}(x, y) dA,$$

Another important concept is covariance, which shows the relationship between two random variables. Indeed, the average of the production of the deviation of X from the mean of X and the deviation of Y from the mean of Y is covariance. This parameter's normalization is the correlation coefficient, which is done by making the constant between -1 and 1. Therefore, the covariance and correlation coefficients are respectively defined as

$$\begin{aligned} Cov(X, Y) &= E((X - \mu_X)(Y - \mu_Y)) = E(XY) - E(X)E(Y) \\ &= \int_{-\infty}^{\infty} \int_{-\infty}^{\infty} xy f_{X,Y}(x, y) dA \\ &\quad - \int_{-\infty}^{\infty} \int_{-\infty}^{\infty} x \cdot f_{X,Y}(x, y) dA \int_{-\infty}^{\infty} \int_{-\infty}^{\infty} y \cdot f_{X,Y}(x, y) dA, \end{aligned}$$

$$\rho_{X,Y} = \frac{Cov(X, Y)}{\sqrt{Var(X)}\sqrt{Var(Y)}} = \frac{\sigma_{X,Y}}{\sigma_X\sigma_Y}$$

As mentioned before, the correlation coefficient has a value between -1 and 1. This value determines the linear relationship between X and Y. In other words, as long as the absolute value of this constant is close to one, a strong linear relationship between two random variables can be considered. The marginal distributions can be defined by the integrals and can also be assumed as a PDF of X and Y. Thus, the following definitions for marginal distribution with respect to X and Y, can be considered respectively as

$$h_X(x) = \int f_{X,Y}(x, y) dy, \quad g_Y(y) = \int f_{X,Y}(x, y) dx$$

X and Y as random variables are independent if the multiplication of marginal distribution functions yields the joint probability distribution. In this case, the covariance of X and Y will be equal to zero. However, the inverse is not correct, i.e., if the covariance of X and Y is equal to zero, then it is not necessary that this

leads to the independence of X and Y. This property is used several times in this thesis.

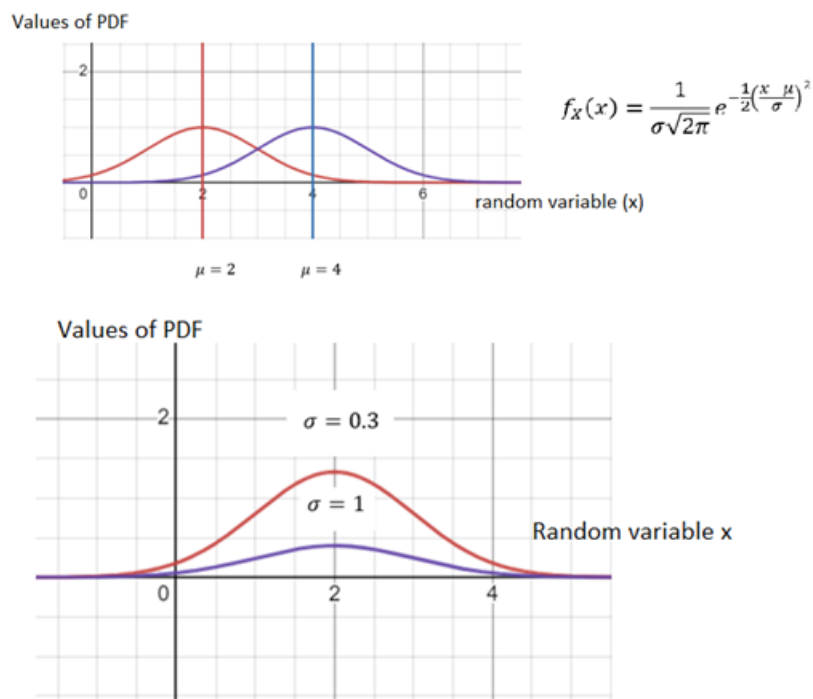
In the study of probability, one may face different distributions with different properties. However, some distributions have the same attitude, and can be unified as a single formula. For example, the bell-shaped functions arise severally in the investigation of PDF. The bell-shaped distribution with a symmetrical shape and maximum at the expected value is called "normal distribution," or more generally, "Gaussian distribution." The given PDF can be formulated as

$$f_X(x) = \frac{1}{\sigma\sqrt{2\pi}} e^{-\frac{1}{2}\left(\frac{x-\mu}{\sigma}\right)^2}$$

In this case,  $\mu$  represents the mean or expected value, and  $\sigma$  represents the standard deviation. The form of this function shows how changes in the value of the mean or standard deviation can affect the behavior of PDF. Indeed, the Gaussian distribution determines a family of bell-shaped distributions with two parameters  $\mu$  and  $\sigma$ . The following figure shows the value of Gaussian PDF with different means and variances:

Figure3.

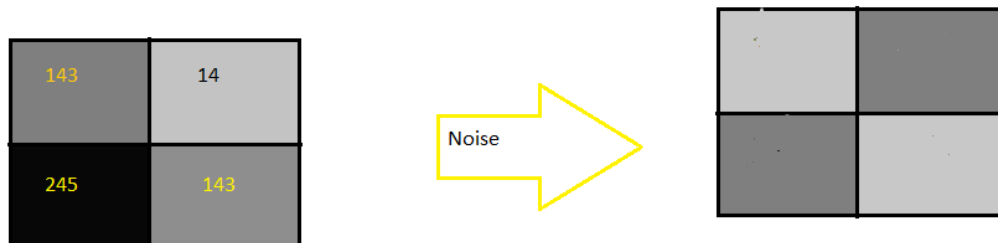
*The Gaussian distribution function with different standard deviations*



Let us now examine the relationship between these distributions and noise. As it mentioned before, the medical images are grayscale, and the noise can affect the gray level of each pixel of the image. In this case, one can think of an original image's pixels as a sample space. Therefore, there is a continuous random variable that determines the level of gray of each point. This number ranges between 0 and 255 in an 8-bit-deep image. In the next figure, the image with 4 pixels is considered, and the effect of noise can be seen as modifying the level of gray for these pixels.

Figure4.

*Windows and gray -level modification*



Based on practical experiments, the likelihood of changing the level of gray of a given pixel can be discussed. The probability of changing the pixel's color can follow the Gaussian distribution. For instance, if the Gaussian distribution with a mean of 145 is assumed, then the probability of the color being affected by noise with the code of 145 (close enough to pure black) is higher than for other colors. In this case, the noise is Gaussian, or that the noise is distributed with Gaussian PDF. Therefore, the distribution function determines the attitude of noise in the original image.

It is remarkable that the noise can affect the original image, and the distribution of  $X$  as a grey level of image can be expressed with different PDFs. To determine the type of distribution of the studied noise, finding the constants of these distributions is necessary. One of these methods will be introduced in the next section. In addition, considering the shape of the distribution and related parameters is important. Another considerable distribution of noise is the Rayleigh distribution, which is named after the British mathematician Lord Rayleigh. The PDF for  $x > 0$  is given as a multiplication of  $x$  as a polynomial with the exponential function. i. e.

$$f_X(x) = \begin{cases} \frac{x}{\sigma^2} \exp\left(-\frac{1}{2}\left(\frac{x}{\sigma}\right)^2\right) & x > 0, \\ 0 & x < 0. \end{cases}$$

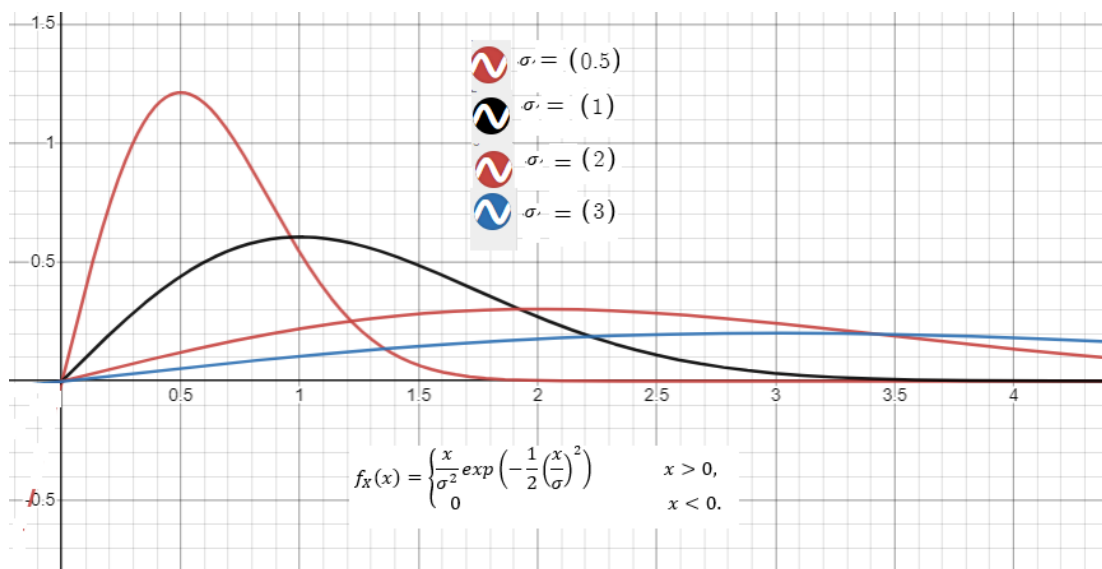
The Rayleigh distribution with different values for  $\sigma$  is plotted in the next figure. For the case  $\sigma = 1$ , the shape is similar to the Gaussian distribution, which is skew-right. In the given figure, the mean is greater than the mode and lies to the left of the mode. The mean and variance can be calculated as follows:

$$E(X) = \int_0^{\infty} x \cdot \frac{x}{\sigma^2} \exp\left(-\frac{1}{2}\left(\frac{x}{\sigma}\right)^2\right) dx = \sigma \sqrt{\frac{\pi}{2}}$$

$$\text{Var}(X) = E(X^2) - (E(X))^2 = \frac{\sigma^2(4 - \pi)}{2}$$

Figure 5.

*Rayleigh distribution with different standard deviations*



This distribution is part of a more general family of distributions named the Weibull distribution. More parameters and variables could be considered to generalize the Rayleigh distribution.

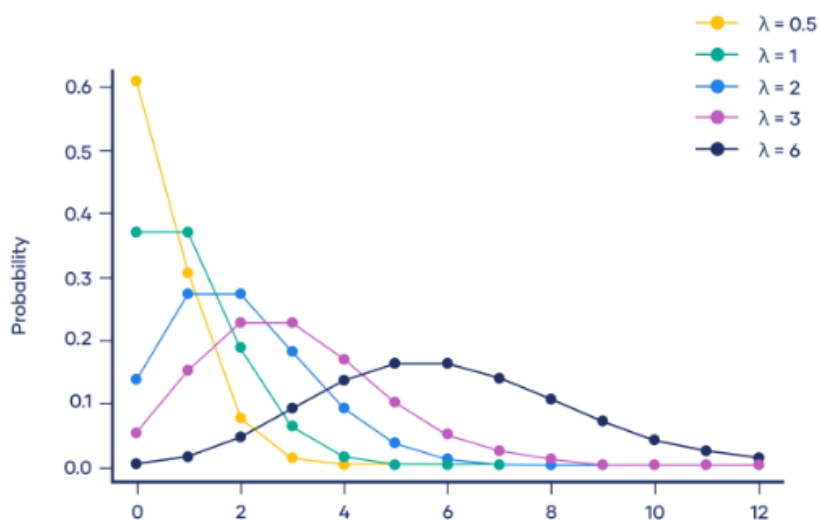
The Poisson distribution is another distribution whose function is important in the study of image noise. This distribution is discrete. However, the continuous type can be generalized and derived from this formula. This function has a parameter called lambda, which describes the mean of the distribution. The PDF of this random variable is given by

$$P(X = x) = f_X(x) = \frac{e^{-\lambda} \lambda^x}{x!}$$

Here,  $x$  follows the Poisson distribution. The discrete outcome is the number of times an event occurs. This distribution is used to predict or explain the number of events occurring within a given interval of time or space. The interval can be any specific amount of time or space, such as 7 square inches or 2 days. The individual events happen at random and independently here, and the random variable should satisfy this condition. The graph of this distribution for different lambdas is sketched in the next figure. The peak of the function describes the most probable number in the figure, which is called the mode. For non-integer lambda, the mode is the closest integer smaller than lambda. For integer lambda, two modes can be considered, and the modes are lambda and lambda minus one. For the big lambda, the attitude of this distribution and the Gaussian distribution will be the same. i.e., for a large enough lambda, the distribution is bell-shaped. Both the mean and variance of this distribution are equal to the parameter lambda. This distribution can be used as an approximation of the binomial distribution as well.

Figure 6.

*Poison distribution with different lambda*



In order to extend the Poisson distribution to the continuous PDF, the factorial of the natural number should be extended. The generalization of the factorial operator of any natural number is the gamma function, which was introduced by Euler. Indeed, different approaches can only yield one unique extension of the factorial function with some specific properties. The definition of the Gamma function is given by

$$\Gamma(x) = \int_0^{\infty} t^{x-1} e^{-t} dt \quad t > 0$$

This function can be generalized to any complex number with a positive real part. Using the integral by part leads to the following interesting property:

$$\Gamma(x + 1) = x\Gamma(x)$$

It is easy to see that  $\Gamma(1) = 1$ , then, by using the recurrence formula, the factorials of natural numbers can be derived. i. e.,

$$\Gamma(2) = 1. \Gamma(1) = 1!, \quad \Gamma(3) = 2. \Gamma(2) = 2!,$$

$$\Gamma(4) = 3. \Gamma(3) = 3!, \dots \Gamma(n) = (n - 1)!$$

After using some trigonometric substitution and applying the polar coordinate in this integral, the value of  $\Gamma\left(\frac{1}{2}\right)$  can be evaluated and  $\Gamma\left(\frac{1}{2}\right) = \sqrt{\pi}$ .

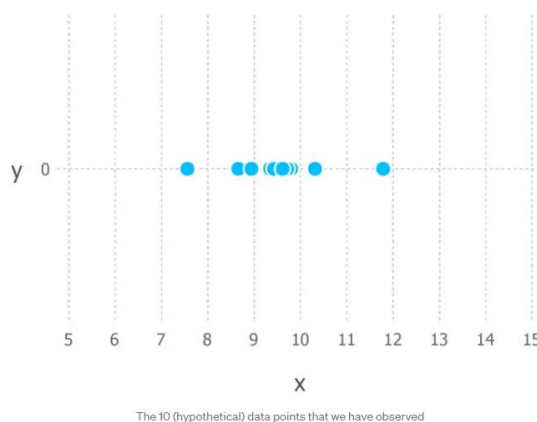
In this section, a few types of PDFs were introduced. However, there are numerous distributions that result from various aspects of research. One critical question is determining the unknown parameters of PDF with the aid of given observations. i.e., if the type of distribution can be estimated, such as Gaussian or Rayleigh, then based on the given observation, find the unknown parameters as the mean or standard deviation. One of the essential methods for finding the parameters of an estimated PDF is MLE, or maximum likelihood estimation, which is introduced in the next section (Bertsekas & Tsitsiklis, 2002).

### **Maximum Likelihood Estimation (MLE)**

In this section, the maximum likelihood estimation method is described and a simple example is investigated to help understand the procedure (Meijer et al., 2019). In the study of noise in image processing, the frequency of noise for different levels of grey can be plotted. This graph shows the frequency of noise for each grey level as a histogram graph. Based on the shape of the distribution, the type of distribution can be approximated. In the next step, the parameters of distribution should be determined. For instance, suppose a simple sampling of 10 observations from some statistical experiment. The following figure shows the dot plot of these observations. Here,  $X$  denotes the random variable, which can be interpreted as noise at the grey level. For instance,  $X = 9$  indicates that noise at grey level is 9. In reality, the number of observations is not that small, of course.

Figure7.

*The dot plot diagram of 10 observations*

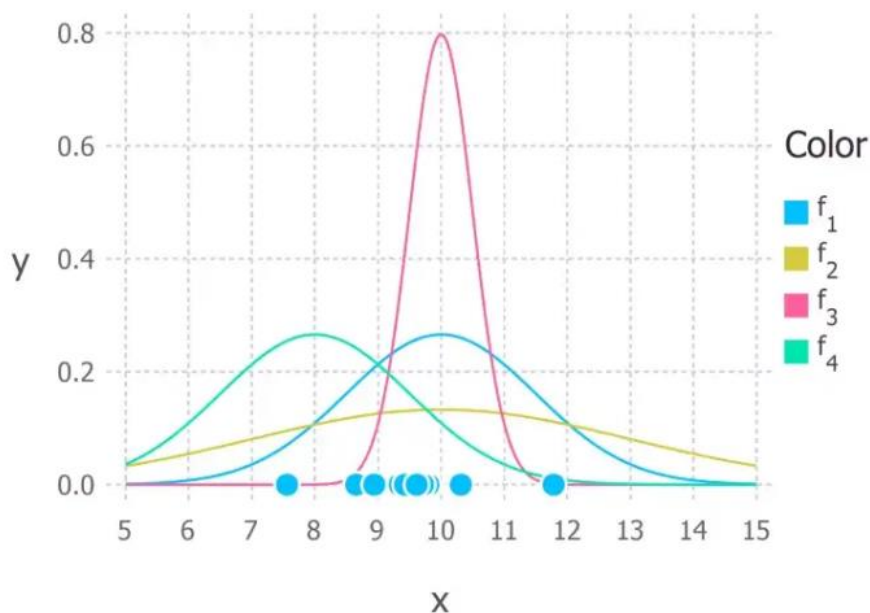


The first step is choosing the model of distribution. This part is very important and crucial. At the very least, it should be clear about the model to utilize. This procedure needs some investigation about the domains of data. The observations can be seen to be accumulated at one specific point, with some scattered values at the right and left sides of the center. This form of distribution suggests the bell-shaped form or Gaussian distribution. However, making this sort of decision on the fly based only on 10 observations is ill-advised, given that the observed values were constructed by a Gaussian distribution.

As it was mentioned before, the Gaussian distribution has two significant factors. The mean and standard deviation of the Gaussian distribution determine the shape of this PDF. The maximum likelihood estimation determines these factors such that the joint probability distribution of observations will be maximized. Here, since there is a produced of values using a Gaussian distribution generator, it can be seen that  $\mu = 10, \sigma = 2.25$ , so  $X \sim N(10, 2.25)$ . (i. e.,  $X$  follows the Gaussian (Normal) distribution with  $\mu = 10, \sigma = 2.25$ .)

Figure 8.

The 10 data points and possible Gaussian distributions from which the data were drawn ( $f_1$  is normally distributed with mean 10 and variance 2.25 this is also denoted  $f_1 \sim N(10, 2.25)$ ,  $f_2 \sim N(10, 9)$ ,  $f_3 \sim N(10, 0.25)$  and  $f_4 \sim N(8, 2.25)$ ). The goal of maximum likelihood is to find the parameter values that give the distribution that maximize the probability of observing the data)



To understand the MLE method, let us examine three different observations with a Gaussian distribution. Assume that the numbers 9, 9.5, and 11 are our observations with a Guamanian distribution. Moreover, assume that they are independent. i.e., their joint probability distribution is the same as the product of their marginal distributions. Therefore, their joint probability distribution can be evaluated as follows:

$$\begin{aligned}
 P(X_1 = 9, X_2 = 9.5, X_3 = 11; \mu, \sigma) & \\
 &= P(X_1 = 9; \mu, \sigma) P(X_2 = 9.5; \mu, \sigma) P(X_3 = 11; \mu, \sigma) \\
 &= \frac{1}{\sigma\sqrt{2\pi}} e^{-\frac{1}{2}\left(\frac{9-\mu}{\sigma}\right)^2} \frac{1}{\sigma\sqrt{2\pi}} e^{-\frac{1}{2}\left(\frac{9.5-\mu}{\sigma}\right)^2} \frac{1}{\sigma\sqrt{2\pi}} e^{-\frac{1}{2}\left(\frac{11-\mu}{\sigma}\right)^2}
 \end{aligned}$$

Now, the mean and standard deviation should be calculated, such that the given joint probability distribution will be the maximum. To find the maximum of this expression, the partial derivative of it can be calculate with respect to the mean and standard deviation and make it equal to zero. In this way, the critical point of this

function can be found. Since the calculation of the derivative with the aid of natural logarithm is simpler, let us calculate the logarithm of both sides.

$$\begin{aligned} \ln(P(x; \mu, \sigma)) &= \ln\left(\frac{1}{\sigma\sqrt{2\pi}}\right) \left(-\frac{1}{2}\left(\frac{9-\mu}{\sigma}\right)^2 - \frac{1}{2}\left(\frac{9.5-\mu}{\sigma}\right)^2 - \frac{1}{2}\left(\frac{11-\mu}{\sigma}\right)^2\right) \\ &= -3\ln(\sigma) - \frac{3}{2}\ln(2\pi) - \frac{1}{2\sigma^2}((9-\mu)^2 + (9.5-\mu)^2 + (11-\mu)^2) \end{aligned}$$

Now if the partial derivative respect to mean is taken then

$$\frac{\partial}{\partial\mu} \ln(P(x; \mu, \sigma)) = \frac{1}{\sigma^2} (9 + 9.5 + 11 - 3\mu)$$

To find the critical point, The derivative should be equal to zero or undefined. Here, making the derivative equal to zero leads to the value of this parameter (mean)

$$\mu = \frac{9 + 9.5 + 11}{3} = 9.833$$

Therefore, the MLE method is used to estimate the parameters of the guessed distribution. As mentioned, the joint probability of given observations can be expressed as a product of their probabilities by summing the independence of random variables. The result will be an equation with unknown parameters, and a partial derivative helps find their critical points. The parameters are found based on maximizing the given joint probability distribution.

Another important issue in the study of noise in medical images is filtering. After determining the type of noise in medical images, the noise should be removed. There are three methods introduced in the next section. The three methods are median filtering, mean filtering, and the combination of these two methods, hybrid filtering.

### **Noise Extraction Methods, Medical Image Filtering Methods**

As it was mentioned before, the noise is a source of interference in medical images. Denoising results in a sharp and clear medical image after extracting the noise. This can be done with the aid of filtering. There are two types of medical image filters based on the format of the filtering function: linear and non-linear (Punarselvam & Suresh, 2019; Denysiuk & Prokopenko, 2020). Despite nonlinear filters, there is a matrix representation for linear or convolution filters. Some

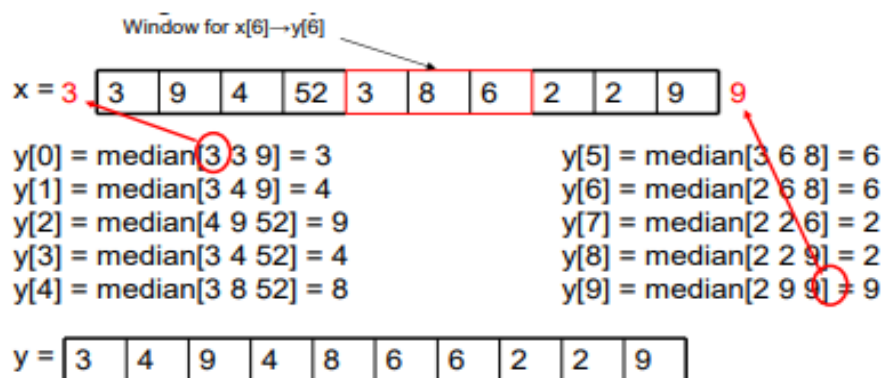
examples of nonlinear filters are threshold, equalization image, and median filters. In this section, the filtering of medical images is studied with some examples.

Median filtering is one of the nonlinear techniques used in medical image filtering to eliminate noise from the images. This technique is popular because it successfully reduces noise while maintaining the edges. It works very well to eliminate "salt and pepper" noise. The median filter operates by going pixel-by-pixel across the image and replacing each value with the median value of nearby pixels. The entire image can be meshed and divided into pixels or slides, yielding patterns known as "windows." A piece of data that is exactly in the middle of an observation when they are sorted is known as its median. In other words, the median is greater than half and less than the rest of the observations. Therefore, the median of the grey level can be computed by sorting the observations of the neighbors into numerical order and replacing them in their place (Erkan et al., 2020).

The following figure determines the procedure of the median filter in an array of 10 observations. The median of a group of three observations in each neighbor is calculated and transformed to the new array. For the initial and terminal values in the array, the beginning observation is repeated to progress the method. There are two distinguishing features in the given figure. First, the given array is in 1-dimension, and extending it to 2-dimensions can be controversial due to the debates on neighbors as 8 pixels. Second, the values of boundaries, which were repeated in the given figure and can be extended and replaced by, for example, 0, or any assumed value.

Figure 9.

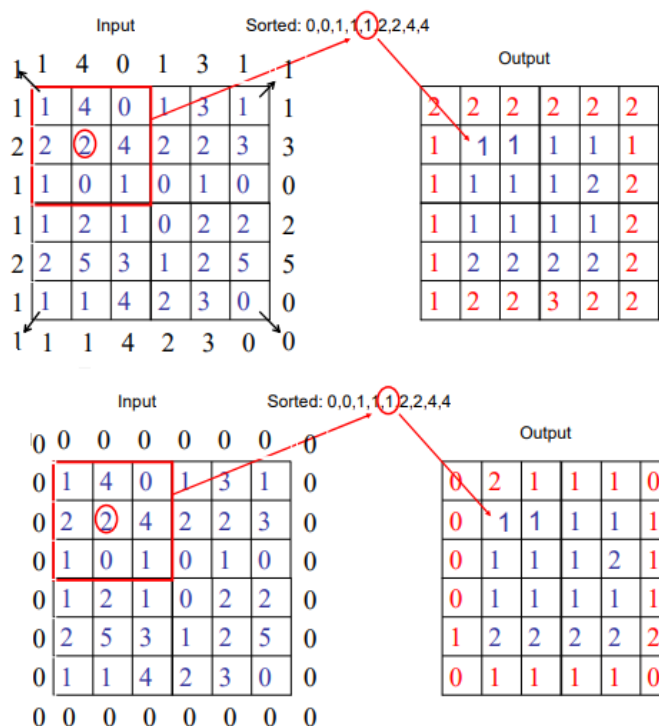
*median filter for the array of observations*



The results for 2D median image filtering with a matrix of 3 by 3 and two different boundary strategies are given in the following figure.

Figure 10.

*median filter for the matrices of observations*



Let us talk about the reason for naming this filter "salt and paper noise removing." At first glance, observations with significantly large or small values in comparison to their neighbors are eliminated. Indeed, the effects of salt (pure white) or paper (pure black) in the original image can be expressed as a window with a significantly large or small value in comparison to its neighbors and are removed by this filter. In contrast with this filter, a "smooth" image can be obtained by equating the values of neighbors. This filter is named the "mean" (or "average") filter. The same procedure should be implemented to lead to the method. i.e., this time the average or mean of the neighbors should be calculated instead of the median, and the output should normalize the intensity variation between neighboring pixels. The following figure shows the effect of this filter on some observed data (Sonali et al., 2019).

Figure 11.  
*mean filter for the matrices of observation*

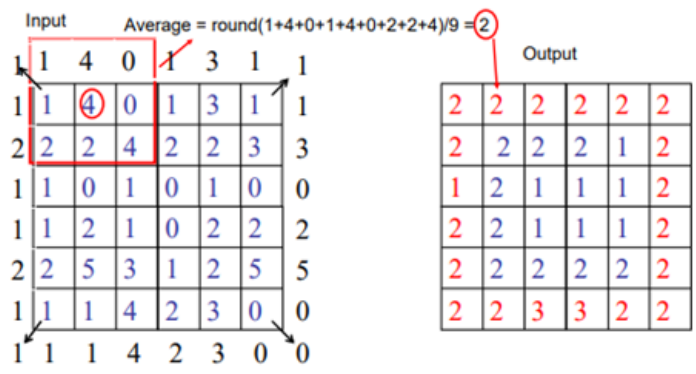


Figure 12.  
*effect of median filter in given image*

### Median Filtering

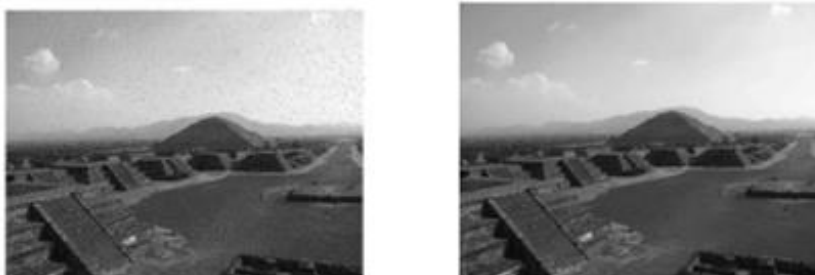


Figure 13.  
*effect of mean filter in given image*

### Average Filtering



Let's fix the value of  $n$ , the dimension of the matrix that would be modified by filtering.  $M_n(\mathbb{R})$  is a set of all square matrices with real numbers as elements. A given set with two operators, i.e., matrix multiplication and the scalar product of real numbers, is a vector space. That means square matrices with the fixed dimension  $n$ , with the given operators, have full-filled properties of vector space. Because  $M_n(\mathbb{R})$  is a vector space, this modification in the values of the matrix can be interpreted as a transformation from  $M_n(\mathbb{R})$  to itself. If the transformation is linear, then it can be represented by a matrix. The noise distribution can be used to express the transformation matrix. Instead of applying the multiplication of matrices in the given vector space, the special multiplication, convolution, could be used. Therefore, many filtering methods arise in the order of noise distribution as Gaussian filters. However, each of these filtering methods, specifically for medical images, has its own advantages and disadvantages. There are many different filtering methods, such as the Sobel filter for edge detection, the Prewitt filter, the hybrid method, which is a combination of the mean and median methods, is used in this thesis. There are many benefits to this choice, such as following the Gaussian distribution due to the central limit theorem.

Roughly speaking, the central limit theorem states that if a sufficiently large number of samples are selected from the population with a mean of  $\mu$  and a standard deviation of  $\sigma$  then the distribution of means of the samples follows the Gaussian distribution with the same mean and standard deviation of  $\frac{\sigma}{\sqrt{n}}$ . Here,  $n$  denotes the number of samples, and repetition is allowed. As a result, if the grey level of pixels in the input images follows any distribution with a mean of  $\mu$  and a standard deviation of  $\sigma$ , then after applying the mean filtering, the distribution of the same random variable follows the Gaussian distribution with the same mean.

The studied model of filtering in this thesis is the hybrid method, which is a combination of mean and median filter methods. The hybrid model determines the required value after applying the median value to the individual pixels in the window. Details of the processing stages are to follow.

The median value is determined by considering an odd-sized rectangular sub-image window. The simple consideration would be to select a sub-image window size of  $3 \times 3$ . The construction of the median filter is completed by taking the vectors within the window and sorting the magnitudes. The operation is repeated by moving

through the image pixel by pixel, and the median value of neighboring pixels replaces the pixel value under consideration. The calculation is performed as follows:

$$Median = median_{(s,t) \in S_{XY}} \{g(s, t)\}$$

The variable  $S_{XY}$  denotes the coordinates in a rectangular sub-image window, and the Median refers to the value of the window.

The sub-image window with coordinates  $S_{XY}$  determines the average and the median values used during the noise removal process. This process improves the accuracy of the pixel values and affects the neighborhood pixels. The moving window enables the total pixel values to be more accurate. The average pixel values can be determined as follows:

$$Average\ value_i = average_{(s,t) \in S_{XY}} \{g(s, t), Median\}$$

The sub-image window is denoted with the variable  $S_{XY}$ , and  $g(s, t)$  represents the pixel values within the sub-image. A subwindow size of  $3 \times 3$  has a total of 9 average pixel values.

The additional accuracy of the hybrid model is due to the use of the mean filter operating on all average values of the sub-image window. The operation adds more accuracy to the pixel values to replace the existing noisy values. The mean pixel values are calculated as follows:

$$Central\ pixel\ value = \frac{\sum_{i=1}^n Average\ value_i}{N},$$

Where  $N = number\ of\ rows \times number\ of\ columns$ .

To compare the accuracy of filter methods, some quantities are defined. One of the most famous scales is the mean square error, or MSE. This quantity describes the average of the square of the absolute error, the difference between the original value and the value after the noise. i. e.,

$$MSE = \frac{\sum (S_{original} - S_{noisy})^2}{n}$$

The square root of the MSE value is denoted by RMSE, and root mean square error is

$$RMSE = \sqrt{MSE}$$

In the end, the peak signal-to-noise ratio, PSNR, is computed based on the maximum number of observations. For instance, the 8-bit image, as mentioned, has a maximum grey level of 255. This value is denoted by  $max$  in the following equation of PSNR:

$$PSNR = 10 \log_{10} \left( \frac{max^2}{MSE} \right) = 20 \log_{10} \left( \frac{max}{RMSE} \right)$$

PSNR is expressed in decibels (dB), which range from 0 to infinity. The image quality is high if the value is high.

## CHAPTER II

### Literature Review

The purpose of a literature review in image noise reduction is to provide an overview and critical analysis of the existing research and methods related to the topic. This review will encompass studies and techniques developed in the field of image processing to address the issue of noise in images, which can significantly impact the quality and interpretation of the image. The literature review will focus on the various types of noise present in images, their sources and characteristics, and the existing methods for reducing or removing them. The review will also provide insights into the advantages, limitations, and evaluation metrics used for assessing the effectiveness of these methods. By conducting a comprehensive literature review, we aim to gain a deeper understanding of the state-of-the-art techniques in image noise reduction and identify potential avenues for future research.

#### Related Works

Some of the related works are briefly described in this section. As mentioned before, medical imaging techniques are used in the diagnosis of many diseases. Medical image processing is essential in making the raw data obtained from imaging techniques meaningful. Current medical image processing technologies are required further investigation. The medical images obtained from different devices can be affected by various noises, and these noises in images are a factor that complicates the diagnosis of the disease (Prabu et al., 2019). Successful noise removal operations are vital for the accurate analysis of medical images and accurate quantitative assessments.

The efficiency of removing noise in images depends on the correct estimation of noise and signal variance. Sijbers & den Dekker (2004) proposed maximum likelihood estimation (MLE), a noise removal method based on the statistical approach. The proposed method estimates the Rician noise level in MRI images.

Baselice et al. (2019) introduced a new method for Rician distribution of noise removal in MRI, the main innovative aspect of the proposed method consists of the criteria adopted for finding similar pixels across the image: it is based on the statistics of the points rather than the widely adopted weighted Euclidean distance.

More in details, the CDF of different pixels are evaluated and compared in order to measure their similarities, exploiting a stack of images of the same slice acquired with different acquisition parameters.

Maza-Quiroga et al. (2021) and Chaudhari & Kulkarni (2021) and Augustin et al. (2022) introduced different methods for the Rician noise distribution where a low signal-to-noise ratio (SNR) exists in MRI applications. The proposed model in Chaudhari & Kulkarni (2021) is derived using the Maximum A Posterior estimator. Noise follows a gaussian distribution at (SNR) ratio and a Rician distribution at low SNR. In the MAP framework, the Gaussian noise model and local statistics of the noisy image are instrumental in the estimation of noise at high SNR. And in the research Augustin et al. (2022) proposed a robust MR image denoising approach based on the concept of memory persistence. Accordingly, improvised and optimized the deep model of memory networks by introducing a data sensitive activation function and a robust cost function, resulting in a compact design with improved noise filtering, feature preservation and enhanced performance.

Karthick & Jayasheela (2021) used a neural network as a probabilistic model to remove the noise in MRI; this research focused on effectively resolving this problem by developing a hybrid classification algorithm of Probabilistic Neural Network whose parameters are optimized using the Firefly Optimization algorithm. In the pre-processing stage, median and wiener filters are used to remove noise, followed by fuzzy clustering by the local approximation of memberships algorithm for segmentation, and finally the gray level co-occurrence matrix and histogram of oriented gradient feature extraction processes.

Recently, Dorjsembe et al. (2022) applied the denoising diffusion probabilistic model to show better performance for noise reduction in MRI.

The analysis of noise distribution was further extended to apply to the single-shot MRI using the segmentation method (Ding et al., 2021). In the research by Ding et al. (2021), they developed a data augmentation method for one-shot brain magnetic resonance imaging (MRI) image segmentation that exploits only one labeled MRI image (named Atlas) and a few unlabeled images. In particular, it is proposed to learn the probability distributions of deformations (including shapes and intensities) of different unlabeled MRI images with respect to the atlas via 3D variational autoencoders (VAEs). In this manner, the research method is able to exploit the learned distributions of image deformations to generate new authentic

brain MRI images, and the number of generated samples will be sufficient to train a deep segmentation network. The research introduced a new standard segmentation benchmark to evaluate the generalization performance of a segmentation network in a cross-dataset setting (collected from different sources).

Sijbers et al. (2007) focus on automatic histogram-based estimation techniques for the estimation of noise variance in the MRI. A new method based on maximum likelihood (ML) is presented. Using Monte Carlo simulation experiments as well as experimental MR data sets, the noise variance estimation methods are compared in terms of the root mean squared error (RMSE). The obtained results show the superiority of the method.

Lili He & Greenshields (2009), it is aimed at estimating the noise-free signal in MRI images. The nonlocal maximum likelihood estimation method (NLME) removes Rician noise in the images. This paper defended that the NLME method used to extract the actual signal from the Rician noise gives optimum results and outperforms MLE.

According to the paper by Rajan et al. (2014), the nonlocal maximum likelihood (NLML) method, which has been successful in removing noise in medical images recently, uses a nonlocal selection of samples and a fixed sample size. This paper proposes an NLML estimation method in which samples are selected by being statistically supported by the Kolmogorov–Smirnov (KS) similarity test. The noise removal performance has been demonstrated by simulating and testing the proposed method with actual data.

Pizurica et al. (2003) proposed the wavelet field method to suppress noise in medical images. The wavelet field estimation approach is based on the joint detection and estimation theory. The proposed algorithm estimates statistical distributions representing useful features and noise in images.

The separation of white Gaussian noise from MRI images is the goal of the research by Sahu et al. (2018) For this purpose, wavelet transform and Bayesian estimator features are used together. MLE and median absolute deviation estimators are used to find noise and signal variances. A probability density function (PDF) is used to obtain the wavelet transform coefficients. The proposed method is based on the statistical modelling of wavelet transform coefficients and is applied to medical images.

Rabbani et al. (2009) proposed a new noise suppression algorithm to improve the image properties of various medical images. The proposed algorithm uses a combination of two variable Laplacian probability density functions. This combination distribution allows for the simultaneous characterization of important statistical features. Various shrinkage functions are obtained using the Maximum a-Posterior (MAP) estimator and the mean square error (MMSE) estimator. An effective noise reduction success for medical images of the proposed method is demonstrated with simulations.

## Chapter III

### METHODOLOGY

#### PROPOSED PROBABILISTIC METHODOLOGY

The goal of this study proposed is to represent actual noise types existing in medical images without requiring knowledge of the source's characteristics. The introduced model creates a probability density function that can successfully depict random varying noise that can be implemented for noise cancellation during real-time processing applications. It combines the existing classical models and provides a facility to represent the noise with less computational complexity accurately. The introduced model uses an exponential base, as in all classical models, and the parameter values are retrieved from the collected data. The parameters give a versatile method for fitting a wide range of noise existing in medical images. Parameter values extracted from the data provide an accurate representation of the noise that classical models cannot fully represent. Another feature of the parameter values is that they represent various types instead of a single type of noise. The exponential function is also of great importance in the introduced probability model. The function is targeted to match the existing probability functions as the parameter values ( $\alpha$ ,  $\beta$ ,  $q$ ) are altered. The probability density function (pdf) can be introduced as an incomplete gamma function that helps the integration function converge. The point to note when using the gamma function is that the result of the integration process must reach the value 1 to satisfy the condition as the probability density function. The stated basic facts help to introduce the statistical probability function as follows.

Definition: Let  $X$  represent an exponentially distributed random variable such that it satisfies  $X \sim GE$

$$f(x; \alpha, \beta, q) = \frac{1}{\Gamma(q+1)} (2\alpha x + \beta)(\alpha x^2 + \beta x)^q \cdot e^{-(\alpha x^2 + \beta x)} \quad (1)$$

Such that  $x > 0$ ,  $\alpha, \beta \geq 0$ ,  $\text{Re}(q) > -1$

Eq. (1) with the parameters  $\alpha, \beta \geq 0$ ,  $\text{Re}(q) > -1$  possess a universal representation for probability density function.

Theorem 1: The function  $f(x; \alpha, \beta, q)$  is the probability density function on  $0 < x < \infty$ .

Proof: The definite integral of the function  $f(x; \alpha, \beta, q)$  over  $0 < x < \infty$  is

$$\begin{aligned} \frac{1}{\Gamma(q+1)} \int_0^{\infty} (2\alpha x + \beta)(\alpha x^2 + \beta x)^q \cdot e^{-(\alpha x^2 + \beta x)} dx \\ = \frac{1}{\Gamma(q+1)} \int_0^{\infty} u^q e^{-u} du \end{aligned} \quad (2)$$

The function  $(\alpha x^2 + \beta x)$  in Eq. (2) is represented as  $u$ . The eq. (2) yields the gamma function as

$$\Gamma(q+1) = \int_0^{\infty} u^q e^{-u} du \quad (3)$$

Substitution of eq. (3) in eq. (2) gives the result as 1, which is sufficient criteria in theory to validate eq. (1) as the probability density function.

It is important to note that the selection of the exponentially distributed random variable  $X$  has some significant properties that represent most classical distributions beyond medical image processing. Some of the exceptional cases are listed below.

If  $X \sim GE\left(\frac{1}{2\alpha^2}, 0, -\frac{1}{2}\right)$ ,  $X$  represents a half-normal distribution

If  $X \sim GE\left(0, \frac{1}{\beta}, 0\right)$ ,  $X$  represents exponential distribution.

If  $X \sim GE\left(\frac{1}{2\alpha^2}, 0, 0\right)$ ,  $X$  represents the Rayleigh distribution.

If  $X \sim GE\left(\frac{1}{\alpha}, 0, \frac{q}{2} - 1\right)$ ,  $X$  represents a generalized gamma distribution.

If  $X \sim GE(\alpha^2, 0, 0)$ ,  $X$  represents the Weibull distribution.

The introduced function in eq. (1) requires the mean  $\mu$ , and variance  $\sigma^2$  relation with the  $\alpha, \beta$  parameters. The relationship can be derived using the theoretical expectation formulation:

$$E(x^2) = \sigma^2 + \mu^2, \quad (4)$$

The expectation of  $\alpha x^2 + \beta x$  can be calculated as

$$\begin{aligned}
 E(\alpha x^2 + \beta x) &= \frac{1}{\Gamma(q+1)} \int_0^{\infty} (2\alpha x + \beta)(\alpha x^2 \\
 &\quad + \beta x)^{q+1} e^{-(\alpha x^2 + \beta x)} (dx) \\
 &= \frac{1}{\Gamma(q+1)} \int_0^{\infty} u^{q+1} e^{-u} du \\
 &= \frac{\Gamma(q+2)}{\Gamma(q+1)}
 \end{aligned} \tag{5}$$

where  $u = (\alpha x^2 + \beta x)$

Eq. (5) produces the following relationship.

$$\alpha(\mu^2 + \sigma^2) + \beta \cdot \mu = \frac{\Gamma(q+2)}{\Gamma(q+1)}. \tag{6}$$

Hoffman & Karst (1975), the authors solved the mean, standard deviation and  $\alpha$  using Rayleigh distribution:

$$\mu = \sqrt{\frac{\pi}{2}} \alpha; \quad \sigma^2 = \alpha^2 \left(2 - \frac{\pi}{2}\right) \tag{7}$$

The eq. (1) also reduces to Rayleigh distribution, and the same process can be applied. Furthermore, the function in eq. (1) can be defined entirely if the moment properties are derived.

The introduced model applies to any randomly varying data satisfying the cumulative distribution function requirements, such as to be bounded below by 0 and bounded above by 1. This has been proved in Theorem 1. The application is not restricted to images but can represent data obtained from various fields. Some typical applications may be the channel loss of wireless communication networks, noise in a radar signal, and noise generated in medical sensors. The model only represents if data is random, not limited between 0 and 1, and not strictly monotonic.

### **Moment Properties**

The moment properties of a function identify the expected variance, the skewness, and the kurtosis. These parameters are sufficient to process eq. (1) in real applications.

Let  $X$  denotes the random variable with pdf of eq. (1). Then the  $n$ th moment of  $X$  can be determined using the confluent hypergeometric function of second kind  $U(a; c; x)$  defined as:

$$U(\alpha, c, x) = \frac{1}{\Gamma(\alpha)} \int_0^{\infty} t^{\alpha-1} (1+t)^{c-\alpha-1} \exp(-x) dt. \quad (8)$$

So

$$E(X^n) = \frac{1}{\Gamma(q+1)} \int_0^{\infty} (2\alpha x + \beta)(\alpha x^2 + \beta x)^q e^{-(\alpha x^2 + \beta x)} (dx). \quad (9)$$

Let  $y$  be a positive function and

$y = \frac{4\alpha(\alpha x^2 + \beta x)}{\beta^2}$ . Then the integral (9) can be written as

$$E(X^n) = \frac{1}{\Gamma(q+1)} \int_0^{\infty} \left(\frac{\beta}{2\alpha}\right)^n (-1 + (1 + y^2)^n \left(\frac{\beta^2}{4\alpha}\right)^q \frac{\beta^2}{4\alpha} e^{-\frac{\beta^2}{4\alpha}y} dy. \quad (10)$$

Recalling the formula

$(f(x) - 1)^n = \sum_{k=0}^n \binom{n}{k} f(x)^k (-1)^{n-k}$ , the integral can be written as

$$E(X^n) = \frac{1}{\Gamma(q+1)} \sum_{k=0}^n \binom{n}{k} (-1)^{n-k} \frac{\beta^{n+2q+2}}{2^{n+2q} \alpha^{n+q+1}} \int_0^{\infty} y^q (1 + y)^{\frac{k}{2}} e^{-\frac{\beta^2}{4\alpha}y} dy. \quad (11)$$

Hence, the  $n$ th moment of the generalized exponential random variable is

$$E(X^n) = \sum_{k=0}^n \binom{n}{k} (1)^{n-k} \frac{\beta^{n+2q+2}}{2^{n+2q} \alpha^{n+q+1}} U\left(q+1, \frac{k}{2} + q + 2, \frac{\beta^2}{4\alpha}\right). \quad (12)$$

It is possible to use the eq. (12) to determine the mean, variance, skewness, and kurtosis.

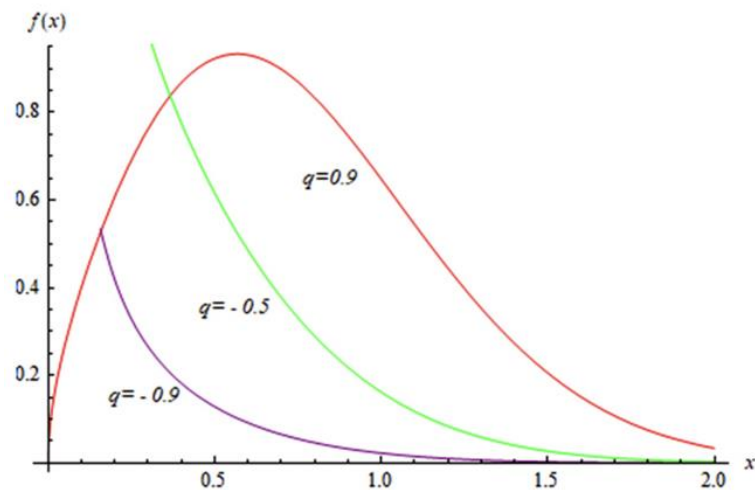
Table1.

Median  $E(X)$ ,  $E(X^2)$  and  $\text{Var}(X)$  of random variable  $X$  for some values of  $\alpha$ ,  $\beta$  and  $q$ .

$\alpha$	$\beta$	$q$	$E(X)$	$E(X^2)$	$\text{Var}(X)$	
<b>0.1</b>	0.1	0.1	0.9	3.62027	15.379	2.27338
		0.5	-0.9	0.158051	0.20974	0.18476
	0.5	0.1	-0.9	0.340613	0.65938	0.054337
		0.5	0.9	2.35891	7.20546	1.64102
<b>0.5</b>	0.1	0.1	0.9	1.72978	3.45404	0.4619
		0.5	-0.9	0.112933	0.08706	0.07431
	0.5	0.1	-0.9	0.181403	0.16371	0.13081
		0.5	0.9	1.40423	2.39577	0.42391
<b>1</b>	0.1	0.1	0.9	1.2427	1.77573	0.23142
		0.5	-0.9	0.092539	0.05373	0.04516
	0.5	0.1	-0.9	0.134691	0.08653	0.06838
		0.5	0.9	1.06961	1.36519	0.22112
<b>2</b>	0.1	0.1	0.9	0.888672	0.90556	0.11582
		0.5	-0.9	0.0736988	0.03157	0.02614
	0.5	0.1	-0.9	0.988766	0.04505	0.03527
		0.5	0.9	0.798308	0.75042	0.11312

Figure 14.

Characteristic plots



Furthermore, one needs to show the robustness of the parameters. Therefore, arbitrarily selected  $\alpha$ ,  $\beta$ , and  $q$  values are tested using eq. (12), and the results are listed in Table 1.

The results in Table 2 show the selected fixed values of  $\beta$  and  $q$ , the first two moments, and  $X$ 's variance decreases as  $\alpha$  increases. The same can be said for any

other parameters. The other important point is that for any fixed value of  $\alpha$  and  $\beta$ , increasing the value of  $q$  also increases the  $E(X)$ ,  $E(X^2)$  and the  $\text{Var}(X)$ .

The characteristic of eq. (1) examined with the selected parameter values of  $\alpha$  and  $\beta$ , with varying values of  $q$ . Results are plotted in Fig. 13.

The plots in Fig. 1. indicate convergence for eq. (1) for all values of  $q$ .

Parameter values derived directly from the data increase the convergence of the function to classical methods and their success. A possible processing method may be to extract parameter values using the probability expectation process and apply Kolmogorov- Smirnov (K-S) theorem to achieve  $\text{Re}(q) > -1$ . This method employs a hybrid process that reduces the sensitivity of parameter values. Therefore, a well-known maximum likelihood estimation method was applied to derive all parameters  $\alpha$ ,  $\beta$ , and  $q$  within the same workspace.

The next task is to extract the parametric values for  $\alpha$ ,  $\beta \geq 0$ ,  $\text{Re}(q) > -1$  as stated in Eq. (1). The calculation process uses the maximum likelihood estimation method to discover the accurate parametric values. The parameter extraction process solves the mathematical differential equations generated by the log-likelihood function of  $L(\alpha, \beta, q)$ . The extension of random data values of  $X$  from 1 to  $n$  such that  $X \sim \text{GE}(\alpha, \beta, q)$  defines the log-likelihood function as:

$$L(\alpha, \beta, q) = -n \ln(\Gamma(q + 1)) + \sum_{i=1}^n \ln(2\alpha x_i + \beta) + \sum_{i=1}^n \ln(\alpha x_i^2 \beta x_i)^q - \sum_{i=1}^n \ln(\alpha x_i^2 \beta x_i) \quad (13)$$

The unknown parameter values of  $\alpha$ ,  $\beta$ , and  $q$  can be determined by differentiating eq. (13) for each unknown parameter as:

$$\frac{\partial L}{\partial \alpha} = \sum_{i=1}^n \frac{2x_i}{2\alpha x_i + \beta} + \sum_{i=1}^n \frac{qx_i}{\alpha x_i + \beta} - \sum_{i=1}^n x_i^2, \quad (14)$$

$$\frac{\partial L}{\partial \beta} = \sum_{i=1}^n \frac{1}{2\alpha x_i + \beta} + \sum_{i=1}^n \frac{q}{\alpha x_i + \beta} - \sum_{i=1}^n x_i, \quad (15)$$

$$\frac{\partial L}{\partial q} = -n \frac{\Gamma'(q + 1)}{\Gamma} (q + 1) + \sum_{i=1}^n \ln(\alpha x_i^2 \beta x_i) = 0 \quad (16)$$

The solution of eq. (14), (15), and (16) yield the parameter values of  $\alpha$ ,  $\beta$ , and  $q$  that can be substituted into eq. (1) to represent the probability density function of random data.

The introduced probability density function can theoretically be verified using the statistical moment properties. The variable  $X$  denotes the random variable as stated in eq. (1). The confluent hypergeometric function of the second kind can be stated as eq. (17).

$$U(a, c, x) = \frac{1}{\Gamma(a)} \int_0^{\infty} t^{a-1} (1+t)^{a-1} e^{-x} dt \quad (17)$$

So that eq. (18) can be defined as:

$$E(x^n) = \frac{1}{\Gamma(q+1)} \int_0^{\infty} x^n (2\alpha x + \beta)(\alpha x^2 + \beta x)^q \cdot e^{-(\alpha x^2 + \beta x)} dx \quad (18)$$

Simplify eq. (18) and let  $z = \frac{4\alpha(\alpha x^2 + \beta x)}{\beta^2}$  produce eq. (19)

$$E(x^n) = \frac{1}{\Gamma(q+1)} \int_0^{\infty} \frac{\beta}{2\alpha} (-1 + (1+z)^{\frac{1}{2}})^n \left(\frac{\beta^2}{4\alpha} z\right)^q \frac{\beta^2}{4\alpha} e^{-\frac{\beta^2}{4\alpha} z} dz \quad (19)$$

The eq. (19) is a result of the theoretical formulation given as

$$(f(x) - 1)^n = \sum_{k=0}^n \binom{n}{k} f(x)^k (-1)^{n-k} \quad (20)$$

The introduced model successfully satisfies the process of determining the moments, skewness and shaping parameters. Several classical distributions rely on the shape parameter to indicate the suitable distribution for the data. The Tukey lambda distribution is beneficial for symmetric distributions, and different lambda values indicate one of the classical models such as exact uniform, U-shape, logistic etc. distribution. However, the generally introduced model allows extraction of the most suitable parameters directly from the randomly varying data. Based on the parameter values, the model can reduce to one of the classical distributions within the same work frame.

The accuracy of the calculated parameter values can be tested with various statistical tools. This research uses the most popular statistical tools, such as the Kolmogorov–Smirnov (K-S) and Akaike Information Criteria (AIC) tests.

### The adopted test procedure

Assuming that the probability density function  $F_x(x)$  represents the empirical samples shown as  $E_n(x)$ , it is possible to state the K-S test as in eq. (21).

$$F[\lim_{n \rightarrow \infty} \sup |E_n(x) - F_x(x)| = 0] = 1, \quad (21)$$

for all  $x$ .

The eq. (21) represents the probability function and is known as the Glivenko-Cantelli theorem in the literature. The purpose of the theorem is to verify the fitness of the introduced probability density function to the recorded samples. The critical condition of the test is that the large recorded sample values  $n$  should produce small enough values (between 0 and 1) due to  $|E_n(x) - F_x(x)|$ . The K-S test is generally defined as eq. (22).

$$D_n = \sup |E_n(x) - F_x(x)|, \quad (22)$$

for all  $x$  and  $n$ .

The testing procedure of eq. (22) includes some critical steps that need to be explained in detail.

The following algorithm is to explain the details of the practical test procedure.

Step 1: The initial step is to define the generated function in Eq. (1).

Step 2: Solve the three equations with three unknowns, eq. (14, 15, 16) to produce parameter values for  $\alpha$ ,  $\beta$ , and  $q$ .

Step 3: Substitute the parameter values in eq. (1).

Step 4: Calculate the cumulative distribution of the proposed and the theoretical functions using the recorded medical image noise. The results are plotted on the same graph for visual comparison.

Step 5: The scientific validity of the proposed method is tested with both the K-S and the AIC tests.

Step 6: The critical and necessary conditions for both tests are verified.

Step 7: The performance analysis tools Root mean squared error (RMSE), relative error (RE), and R-squared error ( $R^2$ ) are used to evaluate the accuracy.

Step 8: Results were tabulated.

The K-S test uses a critical value evaluation as a necessary condition. There are different formulations to use depending on the sample size. The recorded noise data was more than 50. Therefore, the stated formula can be used as follows:

$$\text{Critical value} = \frac{1}{\sqrt{n}} = \frac{1}{\sqrt{80}} = 0.112$$

The prime check is to evaluate eq. (22) to determine  $D_n$  and compare the value with 0.112. The most suitable fitting distribution has the lowest value of  $D_n$ .

The quality of the distributions can further be tested with several methods. This research paper uses the AIC method to justify the goodness of fit and allows a relative test between the distributions.

The AIC test was applied to justify the results obtained with the K-S method. The AIC method is a personal selection, and any other goodness of fit test can be used for such an application. AIC test estimates the quality of each distribution model relative to each other. The AIC formulation is defined as:

$$AIC = 2k - 2Ln(L)$$

The variable k denotes the number of parameters used in the model L denotes the highest value of the likelihood function under test. The lowest value of the AIC test is classified as the most suitable distribution function.

The algorithmic steps in section Moment Properties can be followed quickly with the flowchart in Figure. 15.

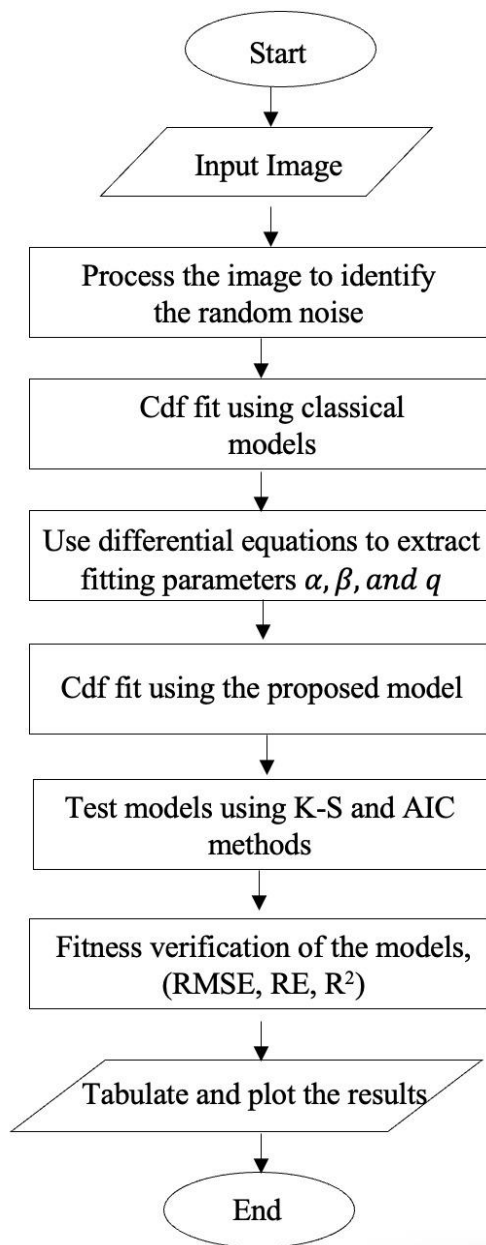
**Figure 15.***Flowchart representation*

Figure 15 is the implementation of the algorithm for the proposed model. The processing part is the same for both the theoretical and the proposed model. The results are tabulated, and scientific performance evaluations are tabulated. The noise was extracted from real medical images.

## Chapter IV

### RESULTS

Noise is an important factor that degrades the quality of radiographs and is known as the random change in the optical density of the image, that is, it can also be expressed as fluctuations in the optical density.

Radiologists have difficulties with image noise in all modalities since it might mislead clinicians when making diagnoses. For soft tissue lesions, for example, form, margin features, and overall density are crucial distinguishing factors between benign and malignant lesions. Number, shape, and distribution of calcifications are crucial aspects to take into account while interpreting them. Therefore, the depiction of the anatomical structure's characteristics, such as contrast, can affect the visibility of soft tissue lesions, whereas the presence of noise, such as random quantum noise, usually limits the visibility of small structures, can affect the detectability of calcifications. However, the ability to distinguish between benign and malignant soft tissue lesions may also be limited by an image's relative increased noise level brought on, for instance, by a lower radiation dosage. Given the connection between these image quality characteristics and the image acquisition process, image quality problems like relatively higher noise levels may be the result of poor acquisition settings, poor automatic exposure control settings, or issues with the system's x-ray.

The noisy image filtered using a hybrid model. This model successfully separates the random noise from the medical image. The performance of the proposed hybrid model can be determined by calculating the RMSE, SNR, and PSNR values. The comparison has been made with classical mean, median, and midpoint filters. The results are listed in Table 2.

Table 2.

*Comparison results.*

<b>Filtering method</b>	<b>SF</b>	<b>MF</b>	<b>MPF</b>	<b>HFM</b>
<b>MR brain image</b>				
<b>SNR (dB)</b>	3.81	3.71	3.6	3.8
<b>PSNR (dB)</b>	43.43	43.64	42.08	43.68
<b>RMSE</b>	441.58	431.33	515.75	429
<b>Abdominal CT image</b>				
<b>SNR (dB)</b>	5.58	5.26	4.06	5.53
<b>PSNR (dB)</b>	19.67	19.79	19.26	27.78
<b>RMSE</b>	26.48	26.12	27.78	25.66

The results in Table 2 demonstrate the success of the hybrid model. It has lower RMSE, higher values of SNR, and PSNR to verify its superiority over the other methods.

It is worth studying the histogram graph and its properties in different sections. Roughly speaking, the histogram is a graphical presentation of data points organized into user-specified ranges. The histogram, which resembles a bar graph in appearance, condenses a data series into an intuitive visual by collecting numerous data points and organizing them into logical ranges or bins. The histogram graph determines the frequencies of observations, and in our case, the X values denote the level of grey color and Y determines the frequency of repetition in the noise effect. In this situation, the discrete forms of data, as a sample, can be formed into a similar continuous distribution if the number of samples is considerable.

The hybrid model applied to various medical images for generalization purposes. The random noise data fitted with the introduced generalized probabilistic distribution function. To test the generalized probabilistic distribution function, several samples of different medical devices from different parts of the body were selected.

The first sample is the image of the panoramic radiography machine. A two-dimensional dental x-ray examination called as panoramic radiography, commonly known as a panoramic x-ray, captures the complete mouth in a single image, including the teeth, upper and lower jaws, surrounding structures, and tissues. The

jaw has a curved shape like a horseshoe. The curving structure, though, appears flat in the panoramic x-ray, like figure 16. Usually, it gives specifics about the teeth and bones.

The proposed distribution function was tested with a selected sample in Figure 16 the histogram of the random noise is plotted in Figure 17, and the cumulative distribution functions are applied to compare the performance of the introduced distribution function in Figure 18.

**Figure 16.**

*Oral panoramic radiograph image*



**Figure 17.**

*Histogram of the random noise in OPG*

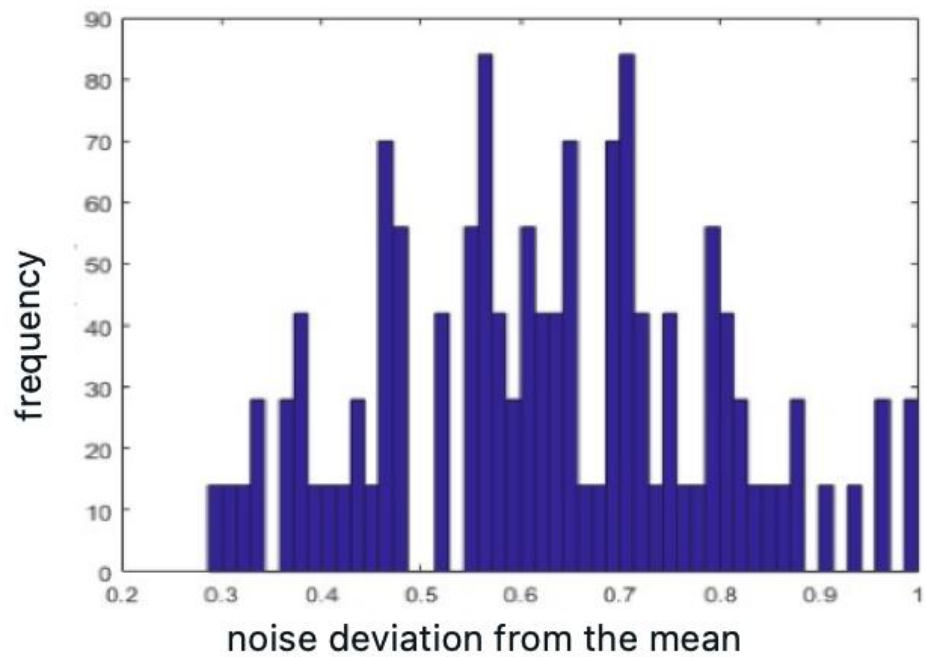
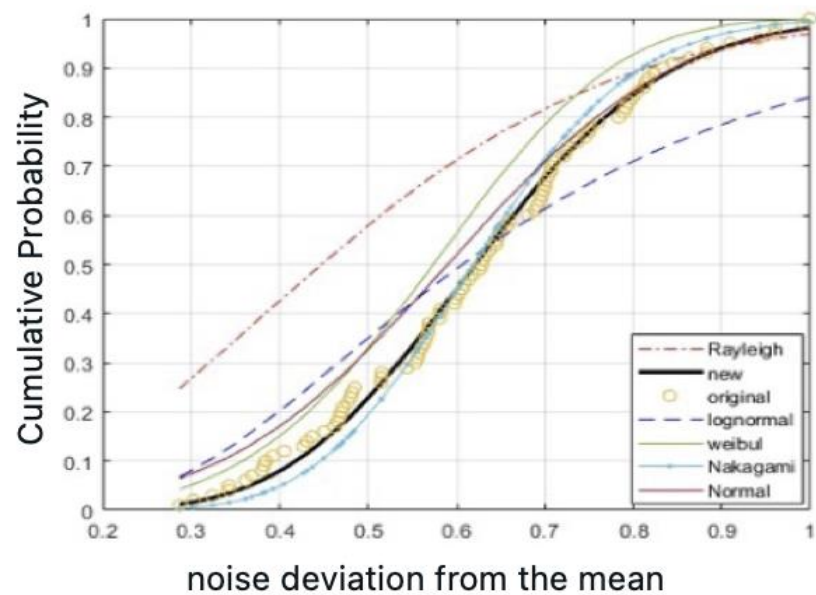


**Figure 18.**

*Comparison of the distribution plots of the OPG image*



The plots in Figure 18 show the proposed model to be the most suitable to represent the noise in such medical images. The parameter values are:

$$\alpha = 2.3198$$

$$\beta = 1.7930$$

$$q = 0.087$$

The scientific validity of the generated function was carried out with the K-S and the AIC tests. The test results are listed in Table 3.

Table 3.

*The goodness-of-fit test results of the oral panoramic radiograph image*

<b>Statistical Model Name</b>	<b>K-S Test</b>	<b>AIC</b>
<b>New</b>	0.0504	96.6825
<b>Normal</b>	0.1275	108.8812
<b>Weibull</b>	0.1527	163.6614
<b>Rayleigh</b>	0.3541	175.6832
<b>Nakagami</b>	0.0874	208.9138
<b>LogNormal</b>	0.1663	298.5882

The introduced model produces the lowest value in the fit. Therefore, using the K-S and the AIC tests confirms the applicability of the introduced model.

The second, third, and fourth samples are used from MRI images. A magnetic field and radio waves produced by a computer are used in the MRI device, a type of medical imaging method, to provide accurate images of the body's organs and tissues. Breast cancer, brain tumours, abnormalities in the spinal disk, bone infections, rotator cuff tears, and other disorders can all be found using an MRI.

In the second sample, brain MRI images were selected. Brain imaging is very important because it can aid medical professionals in their search for disorders like bleeding, swelling, issues with how the brain evolved, tumours, infections, inflammation, damage from an accident or a stroke, or blood vessel issues. The MRI can aid medical professionals in their search for headache or seizure reasons. The noise in the MRI image representing the human brain in Figure 19 is filtered, the histogram of the random noise is plotted in Figure 20, and the comparison of the distribution is plotted in Figure 21.

Figure 19.

*MR image of human brain*

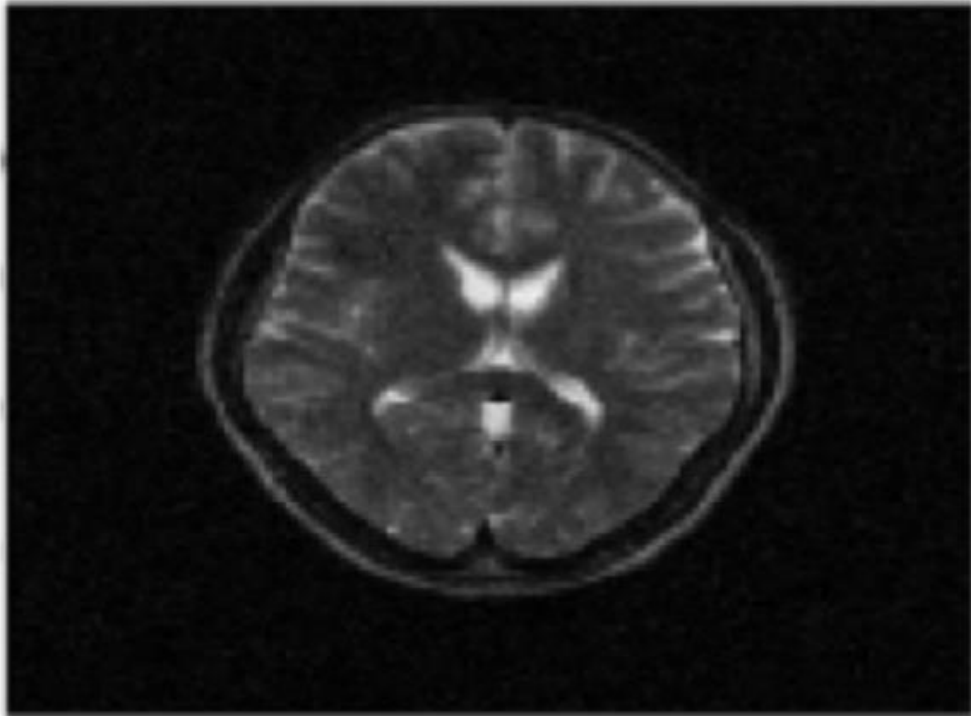


Figure 20.

*Histogram of the random noise in MR image of human brain*

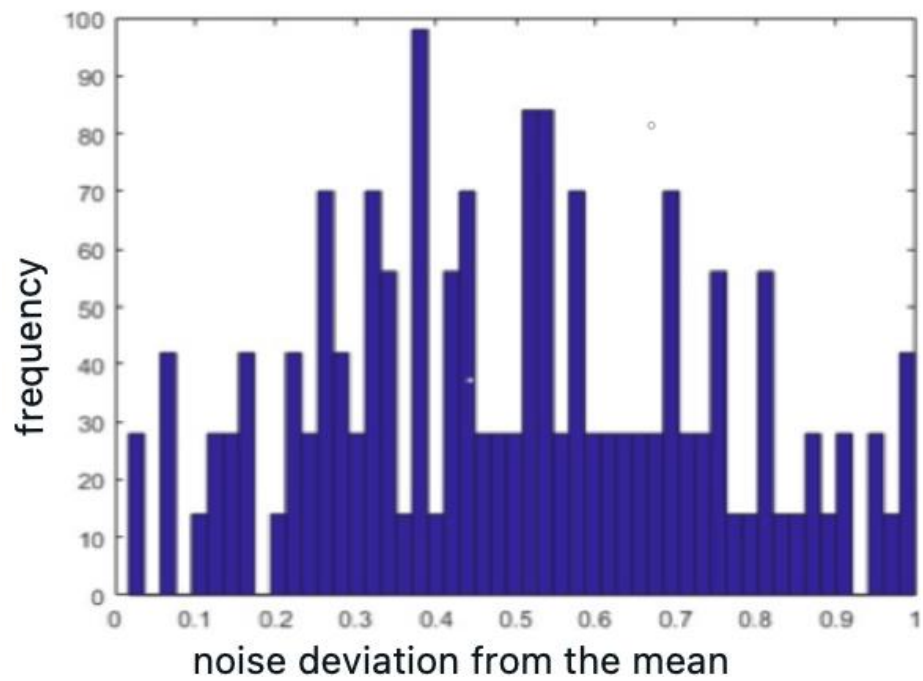
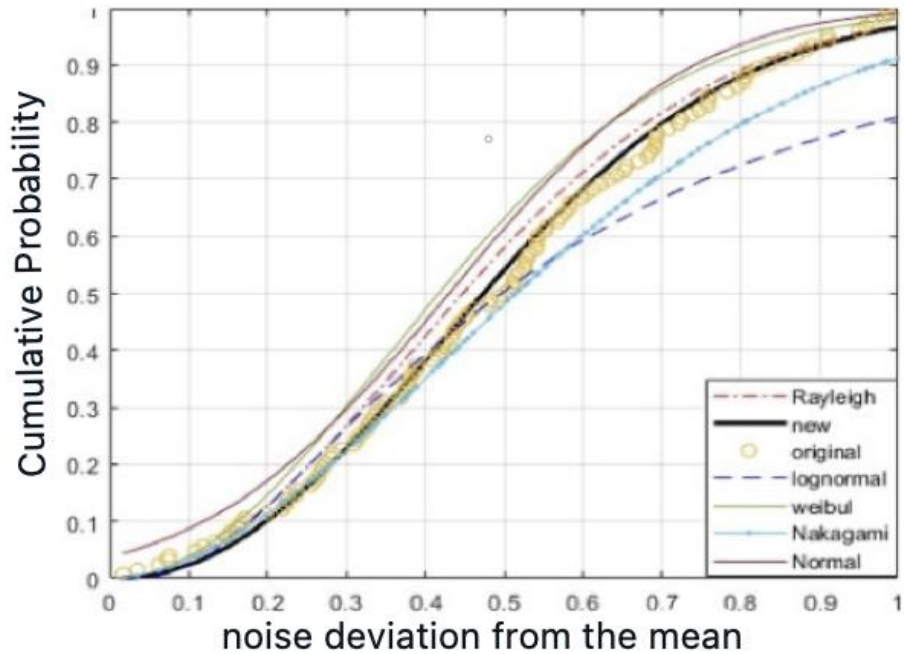


Figure 21.

*Comparison of the distribution plots of the MR image of human brain*



The histogram plot does not indicate a suitable probability distribution function. The proposed and classical distribution functions are computed and plotted in Figure 21 and show the proposed distribution function to be the most suitable model for this test. The parameter values are extracted from the noise data as follows:

$$\alpha = 3.1833$$

$$\beta = 1.9223$$

$$q = 0.9829$$

The validity of the proposed model was carried out with the K-S and AIC tests. The test results are listed in Table 4.

Table4.

*The goodness-of-fit test results of the MR image of human brain*

<b>Statistical Model Name</b>	<b>K-S Test</b>	<b>AIC</b>
New	0.0363	2.1621
Normal	0.1200	12.0259
Weibull	0.1366	22.1061
Rayleigh	0.0902	10.2718
Nakagami	0.0882	6.7303
LogNormal	0.1910	30.2558

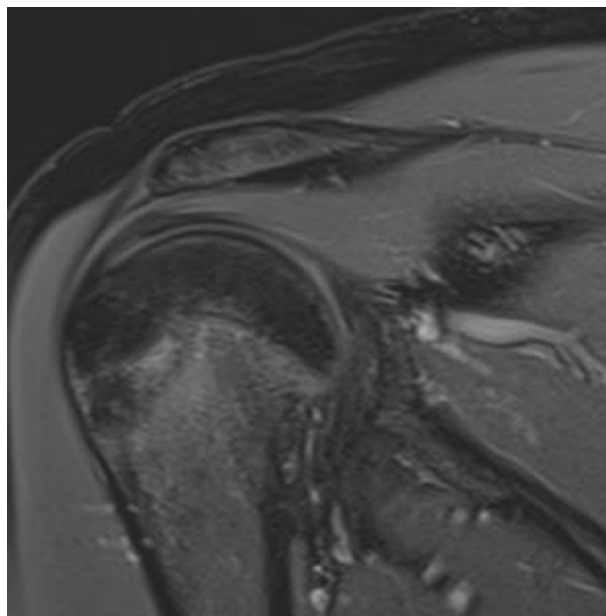
The K-S and the AIC test results in Table 4 indicate the proposed model to be the best among the others.

The third and fourth samples were selected from the shoulder images of MRI devices. These images are controlled by a radiologist and an orthopedic specialist in order to confirm the diagnosis of a rotator cuff tear. For these reasons, two images were selected: a healthy image and a pathological image.

The proposed distribution function was tested with an MRI healthy shoulder image in Figure 22. The histogram plot in Figure 23 represents all recorded random variations. The plots do not indicate the most suitable cumulative distribution type to apply. The cumulative distribution functions are applied to compare the performance of the introduced distribution function in Figure 24.

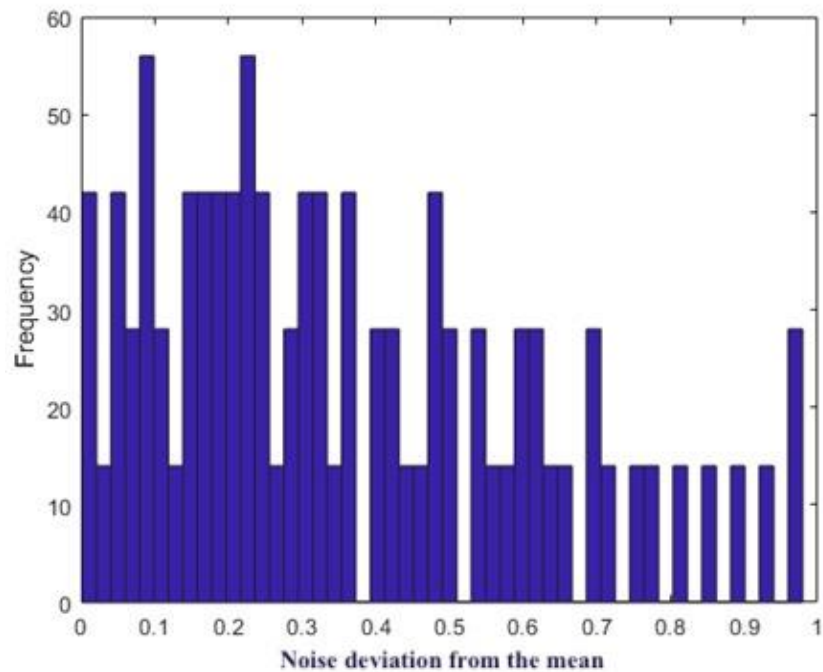
**Figure 22.**

*MR healthy shoulder image*

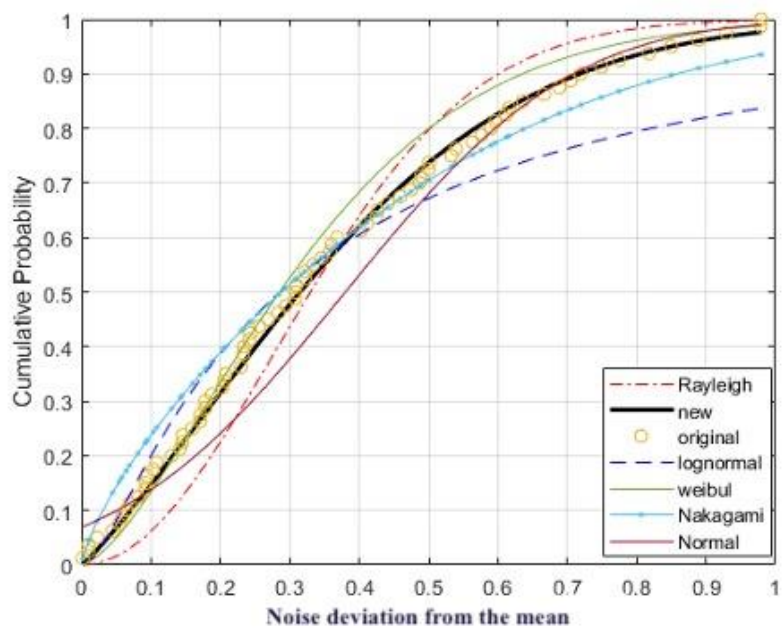


**Figure 23.**

*Histogram of the random noise in MR healthy shoulder image*

**Figure 24.**

*comparison of the distribution plots of the MR healthy shoulder image*



The plots in Figure 24 show the proposed distribution function to be the most suitable for such an application. The parameter values are derived as:

$$\alpha = 2.1188$$

$$\beta = 1.5920$$

$$q = 0.065$$

The scientific validity of the generated function was tested using the K-S and the AIC tests. The test results are listed in Table 5.

**Table5.**

*The goodness-of-fit test results of the MR shoulder image*

<b>Statistical Model Name</b>	<b>K-S Test</b>	<b>AIC</b>
New	0.0402	94.5821
Normal	0.1365	106.7610
Weibull	0.1618	172.5523
Rayleigh	0.3661	182.5725
Nakagami	0.0886	203.7026
LogNormal	0.1765	286.3674

The introduced model produces the lowest value in the fit. Therefore, using the K-S and the AIC tests verify the application of the introduced model.

The proposed model was further tested with a clinical MRI of the pathological shoulder image in Figure 25 the histogram plot in Figure 26, and the cumulative distribution functions in Figure 27.

Figure 25.

*Pathological shoulder MRI image*

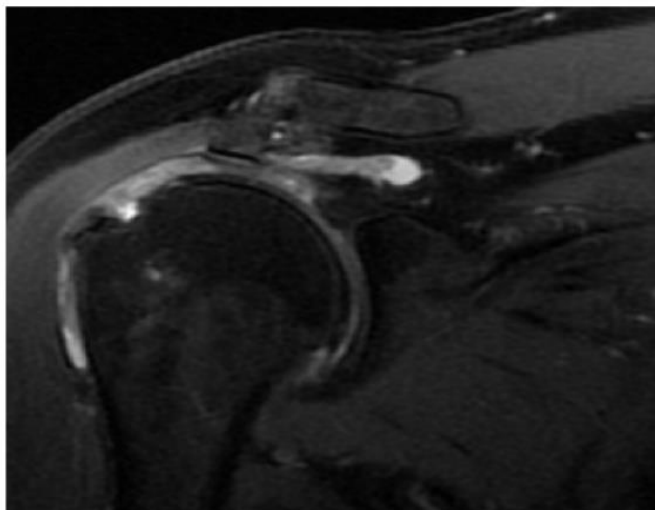


Figure 26.

*Histogram of the random noise in pathological shoulder MRI image*

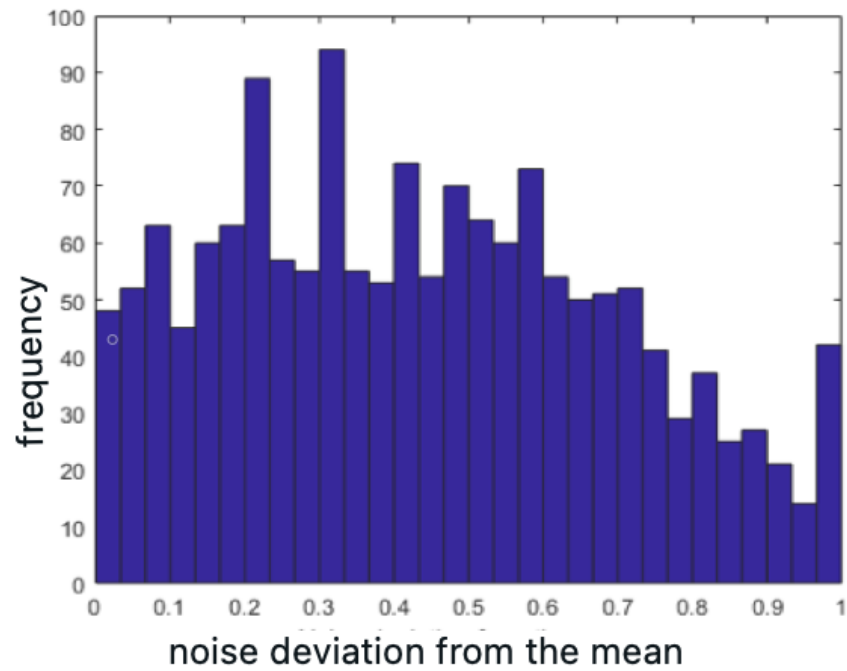
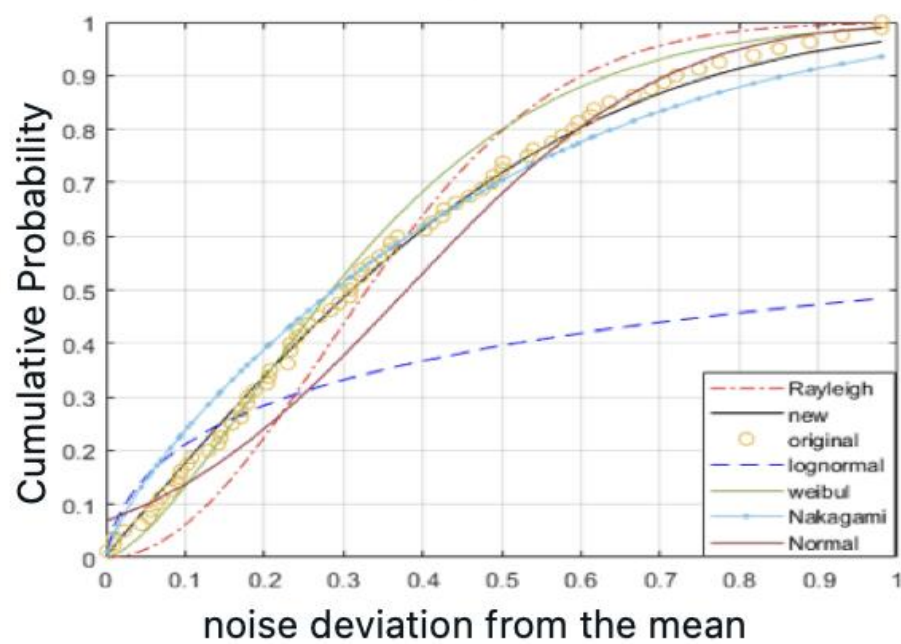


Figure 27.

*comparison of the distribution plots of the pathological shoulder MRI image*



The plots in Figure 27 show the proposed model to be the most suitable to represent the noise in such medical images. The parameter values are:

$$\alpha = 2.2525$$

$$\beta = 0.0070$$

$$q = 0.5095$$

The scientific validity of the generated function was carried out with the K-S and the AIC tests. The test results are listed in Table 6.

**Table 6.**

*The goodness-of-fit test results of the pathological shoulder MRI image*

<b>Statistical Model Name</b>	<b>K-S Test</b>	<b>AIC</b>
<b>New</b>	0.0505	93.4731
<b>Normal</b>	0.2870	105.6350
<b>Weibull</b>	0.1838	170.2183
<b>Rayleigh</b>	0.4052	191.9412
<b>Nakagami</b>	0.0923	202.3146
<b>LogNormal</b>	0.1565	292.4635

The introduced model once again produces the lowest value in the fit. Therefore, using the K-S and the AIC tests confirms the applicability of the introduced model.

The last sample was chosen from the CT device. CT is a type of imaging that creates cross-sectional images of the body using x-rays. Measurements of the attenuation coefficients of x-ray beams passing through the volume of the object under study are used to reconstruct cross-sections. CT imaging is also useful for:

Diagnosing skeletal and muscular conditions, such as bone cancer and fractures. Determine the location of a tumour, infection, or blood clot.

Help with surgical, biopsy, and radiation therapy procedures.

Detect and monitor for diseases and conditions like cancer, heart disease, lung nodules, and liver masses.

Monitor the effectiveness of specific treatments, such as cancer treatment

Identify internal bleeding and injuries.

The proposed model was further tested using an abdominal CT image in Figure 28. The histogram plot is shown in Figure 29. The random noise from the abdominal CT image fits used classical, and the proposed cumulative distribution functions are plotted in Figure 30.

**Figure 28.**

*Abdominal CT image*

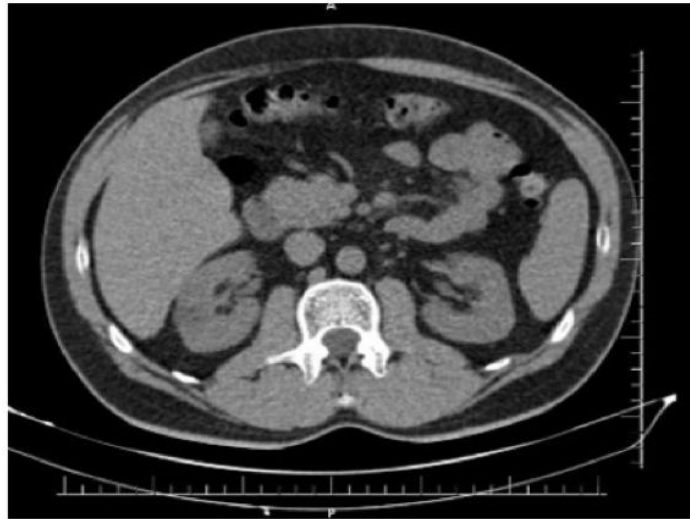


**Figure 29.**

*Histogram of the random noise in the abdominal CT image*

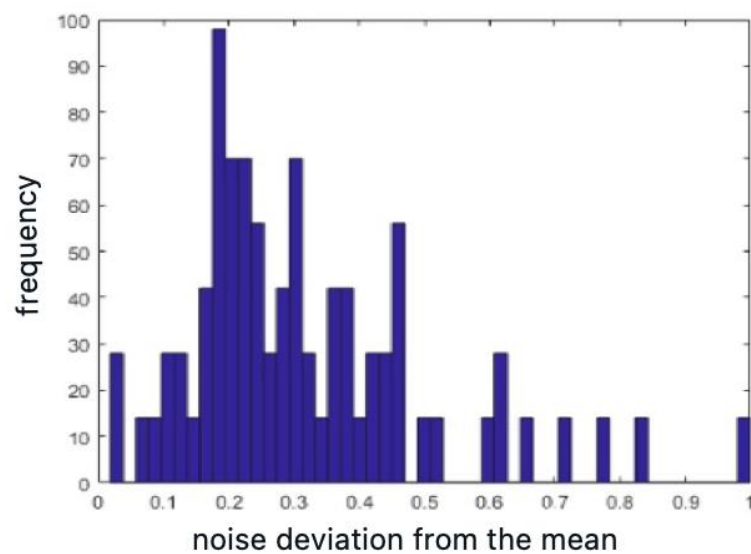
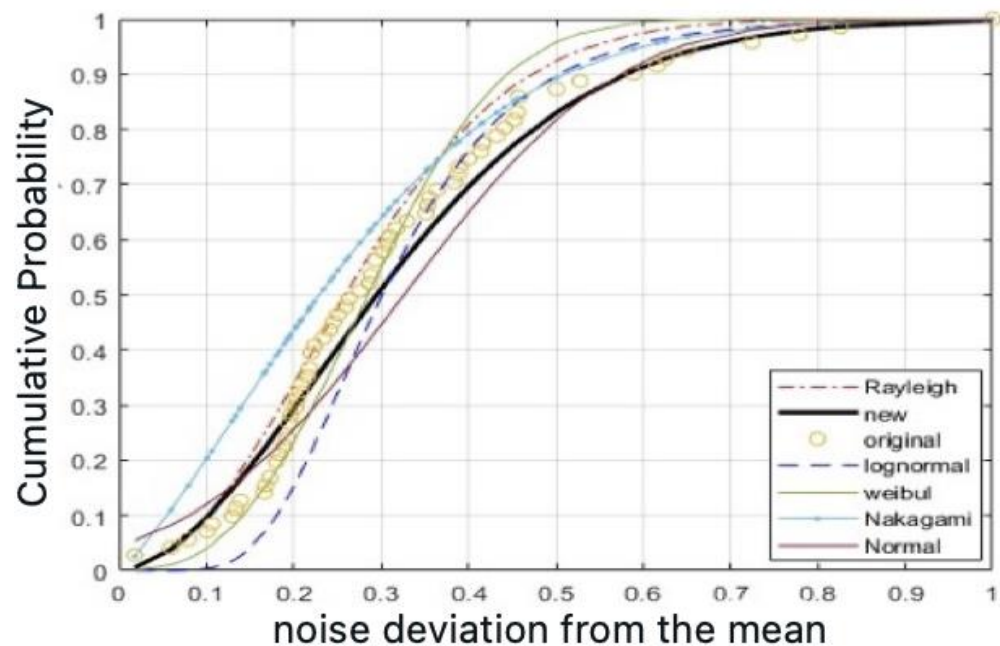


**Figure 30.**

*comparison of the distribution plots of the abdominal CT image*



The plots in Figure 30 show the proposed distribution function favourably applied in the medical image. The extracted parameter values are:

$$\alpha = 4.1366$$

$$\beta = 3.7945$$

$$q = 0.801$$

The scientific validity of the proposed model was determined using the K-S and the AIC tests. The test results are listed in Table 7.

**Table7.**

*The goodness-of-fit test results of the Abdominal CT image*

Statistical Model Name	K-S Test	AIC
<b>New</b>	0.0789	105.1426
<b>Normal</b>	0.1395	145.4564
<b>Weibull</b>	0.1063	134.3499
<b>Rayleigh</b>	0.1063	136.5451
<b>Nakagami</b>	0.2163	151.4718
<b>LogNormal</b>	0.1808	147.4212

The proposed function produces the lowest value in the fit. Therefore, using the K-S and the AIC tests, it is possible to verify the proposed model's applicability to represent the medical image's noise.

### **Validation procedure for the best-fitting model**

The validation procedure helps to evaluate different models under the test. The maximum likelihood estimation method was adopted to calculate the shape and scale parameters for the distribution models. The performance of the distribution models is based on the close representation of the noise data values. The performance of the individual distribution models was evaluated using the statistical analysis tools such as root mean square error (RMSE), relative error (RE) and R<sup>2</sup>.

The performance of the distribution models using the noise data, as in Figure 24, is listed in Table 8.

**Table 8.**

*Fitness verification for the distribution models of the MR shoulder image*

<b>Possible Distributions</b>	<b>RMSE</b>	<b>RE (%)</b>	<b>R<sup>2</sup></b>
<b>Rayleigh</b>	1.6029	1.8778	0.9328
<b>Normal</b>	3.5731	6.4912	0.9443
<b>Nakagami</b>	1.1459	1.4671	0.9707
<b>Weibull</b>	1.8860	5.7903	0.9770
<b>Lognormal</b>	1.3999	7.3367	0.9419
<b>New</b>	0.4212	0.1909	0.9871

The best-performing candidate is the proposed model with RMSE of 0.4212, RE of 0.4101, and R<sup>2</sup> Error of 0.9953 (closest to 1 is the best performance).

The performance was performed further on the data related to Figure 18. The results are listed in Table 9.

**Table9.**

*Fitness verification for the distribution models of the Oral panoramic radiograph image*

<b>Possible Distributions</b>	<b>RMSE</b>	<b>RE (%)</b>	<b>R<sup>2</sup></b>
<b>Rayleigh</b>	3.1431	14.9964	0.8076
<b>Normal</b>	7.4426	10.9925	0.9179
<b>Nakagami</b>	10.2414	14.8770	0.8573
<b>Weibull</b>	8.3480	15.2716	0.8739
<b>Lognormal</b>	18.2340	18.8968	0.5524
<b>New</b>	0.0119	0.4101	0.9953

The results in Table 9 indicate the best-performing distribution as the proposed model.

The introduced model has exponential bases and performs best for the images, including Gaussian, Rayleigh, and Rician type distributions. The analysis of this research article includes images in Chapter I. Test results in Chapter IV support the presented argument. MRI images include mostly Gaussian, Rayleigh, and Rician distributed random noise. The MRI image in Figure16 and Figure18 was tested using two different models. The results prove that the new model is the best distribution for MRI images.

## Chapter V

### CONCLUSION

Medical images are essential to the medical sciences, so their correct readability is imperative. However, image noise negatively affects it in analysis and interpretation. Noise also continuously degrades the readability of images when sent over distances. Therefore, noise analysis and its precise representation are vital. This article analyses the types of noise that may occur in medical images to determine an accurate representation of the random variations. The accurate representation helps to improve the image-capturing devices, filters and wireless channel modelling. The random variation of the noise is examined using statistical tools. The contribution of the proposed model is that it covers most classical probability distribution functions with varying parameters. The parameter values are directly extracted from the recorded data. These parameters allow the introduced function to fit the data better than the classical models. The newly introduced general function can be used successfully on random values, which provides validity for the cumulative distribution function. The model does not require further analysis to test for fitting. It is directly applied to MRI, CT, and panoramic images. The proposed model was compared with the classical models and produced high accuracy with the actual medical images under the test. The model also proved valid scientifically and is promising to be applied in the analysis of medical images.

## References

- Zhou, S. K., Greenspan, H., Davatzikos, C., Duncan, J. S., van Ginneken, B., Madabhushi, A., Prince, J. L., Rueckert, D., & Summers, R. M. (2021). A Review of Deep Learning in Medical Imaging: Imaging Traits, Technology Trends, Case Studies With Progress Highlights, and Future Promises. *Proceedings of the IEEE*, 1–19. <https://doi.org/10.1109/jproc.2021.3054390>
- Chen, X., Wang, X., Zhang, K., Fung, K.-M., Thai, T. C., Moore, K., Mannel, R. S., Liu, H., Zheng, B., & Qiu, Y. (2022). Recent advances and clinical applications of deep learning in medical image analysis. *Medical Image Analysis*, 79, 102444. <https://doi.org/10.1016/j.media.2022.102444>
- Ferdjallah, M., & Barr, R. E. (1994). Adaptive digital notch filter design on the unit circle for the removal of powerline noise from biomedical signals. *IEEE Transactions on Biomedical Engineering*, 41(6), 529–536. <https://doi.org/10.1109/10.293240>
- Sundararaj, V. (2019). Optimised denoising scheme via opposition-based self-adaptive learning PSO algorithm for wavelet-based ECG signal noise reduction. *International Journal of Biomedical Engineering and Technology*, 31(4), 325. <https://doi.org/10.1504/ijbet.2019.103242>
- Devasahayam, S. R. (2019). Signals and Systems in Biomedical Engineering: Physiological Systems Modeling and Signal Processing. In *Google Books*. Springer. [https://books.google.com.cy/books?hl=tr&lr=&id=866PDwAAQBAJ&oi=fnd&pg=PR5&dq=Noise++source+in+biomedical+engineering+&ots=SSoibTiz4Z&sig=LSJV1UYWTJdNy\\_0me6X6hr5ik-M&redir\\_esc=y#v=onepage&q=Noise%20%20source%20in%20biomedical%20engineering&f=false](https://books.google.com.cy/books?hl=tr&lr=&id=866PDwAAQBAJ&oi=fnd&pg=PR5&dq=Noise++source+in+biomedical+engineering+&ots=SSoibTiz4Z&sig=LSJV1UYWTJdNy_0me6X6hr5ik-M&redir_esc=y#v=onepage&q=Noise%20%20source%20in%20biomedical%20engineering&f=false)
- Kher, R. (2019). Signal Processing Techniques for Removing Noise from ECG Signals. *J Biomed Eng Res*, 3, 101. <http://www.jscholarpublishers.com/articles/JBER/Signal-Processing.pdf>
- Mohd Sagheer, S. V., & George, S. N. (2020). A review on medical image denoising algorithms. *Biomedical Signal Processing and Control*, 61, 102036. <https://doi.org/10.1016/j.bspc.2020.102036>
- Prabu, S., Balamurugan, V., & Vengatesan, K. (2019). Design of cognitive image filters for suppression of noise level in medical images. *Measurement*, 141, 296–301. <https://doi.org/10.1016/j.measurement.2019.04.037>

- Karimi, D., Dou, H., Warfield, S. K., & Gholipour, A. (2020). Deep learning with noisy labels: exploring techniques and remedies in medical image analysis. *Medical Image Analysis*, 101759. <https://doi.org/10.1016/j.media.2020.101759>
- Nitta, G. R., Sravani, T., Nitta, S., & Muthu, B. (2019). Dominant gray level based K-means algorithm for MRI images. *Health and Technology*, 10(1), 281–287. <https://doi.org/10.1007/s12553-018-00293-1>
- Kiran, M., Ahmed, I., Khan, N., & Reddy, A. G. (2019). Chest X-ray segmentation using Sauvola thresholding and Gaussian derivatives responses. *Journal of Ambient Intelligence and Humanized Computing*, 10(10), 4179–4195. <https://doi.org/10.1007/s12652-019-01281-7>
- Göreke, V. (2023). A novel method based on Wiener filter for denoising Poisson noise from medical X-Ray images. *Biomedical Signal Processing and Control*, 79, 104031. <https://doi.org/10.1016/j.bspc.2022.104031>
- Heylen, R., Thanki, A., Verhees, D., Iuso, D., De Beenhouwer, J., Sijbers, J., Witvrouw, A., Haitjema, H., & Bey-Temsamani, A. (2022). 3D total variation denoising in X-CT imaging applied to pore extraction in additively manufactured parts. *Measurement Science and Technology*, 33(4), 045602. <https://doi.org/10.1088/1361-6501/ac459a>
- Zhang, Z., & Wang, Z. (2022). Computed Tomography Image Features under Denoising Algorithm for Benign and Malignant Diagnosis of Renal Parenchymal Tumor. *Contrast Media & Molecular Imaging*, 2022, 1–8. <https://doi.org/10.1155/2022/5871385>
- Yu, S., & Muhammed, H. H. (2016). Noise type evaluation in positron emission tomography images. 2016 1st International Conference on Biomedical Engineering (IBIOMED). <https://doi.org/10.1109/ibiomed.2016.7869828>
- Nikolov, N., Makeyev, S., Korostynska, O., Novikova, T., & Kriukova, Y. (2022). Gaussian Filter for Brain SPECT Imaging. *Innovative Biosystems and Bioengineering*, 6(1), 4–15. <https://doi.org/10.20535/ibb.2022.6.1.128475>
- Elaiyaraja, G., Kumaratharan, N., & Chandra Sekhar Rao, T. (2019). Fast and Efficient Filter Using Wavelet Threshold for Removal of Gaussian Noise from MRI/CT Scanned Medical Images/Color Video Sequence. *IETE Journal of Research*, 68(1), 10–22. <https://doi.org/10.1080/03772063.2019.1579679>
- Pankaj, D., D., G., & K.A., N. (2021). A novel method for removing Rician noise from MRI based on variational mode decomposition. *Biomedical Signal Processing and Control*, 69, 102737. <https://doi.org/10.1016/j.bspc.2021.102737>

- Zhang, Q., Liu, C., & He, G. (2022). An Improved Wiener Filter Based on Adaptive SNR MRI Image Denoising Algorithm. *2022 International Conference on Computing, Communication, Perception and Quantum Technology (CCPQT)*. <https://doi.org/10.1109/ccpqt56151.2022.00036>
- Wang, Y., Yuan, C., Jiang, J., Peng, K., & Wang, B. (2022). Photoacoustic/Ultrasound Endoscopic Imaging Reconstruction Algorithm Based on the Approximate Gaussian Acoustic Field. *Biosensors*, *12*(7), 463. <https://doi.org/10.3390/bios1207046>
- Guan, B.-O., Jin, L., Ma, J., Liang, Y., & Bai, X. (2021). Flexible fiber-laser ultrasound sensor for multiscale photoacoustic imaging. *Opto-Electronic Advances*, *4*(8), 200081–200081. <https://doi.org/10.29026/oea.2021.200081>
- Pal, C., Das, P., Chakrabarti, A., & Ghosh, R. (2017). Rician noise removal in magnitude MRI images using efficient anisotropic diffusion filtering. *International Journal of Imaging Systems and Technology*, *27*(3), 248–264. <https://doi.org/10.1002/ima.22230>
- Bertsekas, D. P., & Tsitsiklis, J. N. (2002). *Introduction to Probability*.
- Meijer, D., Veselič, S., Calafiore, C., & Noppeney, U. (2019). Integration of audiovisual spatial signals is not consistent with maximum likelihood estimation. *Cortex*, *119*, 74–88. <https://doi.org/10.1016/j.cortex.2019.03.026>
- Punarselvam, E., & Suresh, P. (2019). Non-Linear Filtering Technique Used for Testing the Human Lumbar Spine FEA Model. *Journal of Medical Systems*, *43*(2). <https://doi.org/10.1007/s10916-018-1148-6>
- Denysiuk, V., & Prokopenko, I. (2020). Synthesis of Linear Filters of Smooth Signals. *2020 IEEE Ukrainian Microwave Week (UkrMW)*. <https://doi.org/10.1109/ukrmw49653.2020.9252653>
- Erkan, U., Enginoğlu, S., Thanh, D. N. H., & Hieu, L. M. (2020). Adaptive frequency median filter for the salt and pepper denoising problem. *IET Image Processing*, *14*(7), 1291–1302. <https://doi.org/10.1049/iet-ipr.2019.0398>
- Sonali, Sahu, S., Singh, A. K., Ghrera, S. P., & Elhoseny, M. (2019). An approach for de-noising and contrast enhancement of retinal fundus image using CLAHE. *Optics & Laser Technology*, *110*, 87–98. <https://doi.org/10.1016/j.optlastec.2018.06.061>
- Prabu, S., Balamurugan, V., & Vengatesan, K. (2019). Design of cognitive image filters for suppression of noise level in medical images. *Measurement*, *141*, 296–301. <https://doi.org/10.1016/j.measurement.2019.04.037>

- Sijbers, J., & den Dekker, A. J. (2004). Maximum likelihood estimation of signal amplitude and noise variance from MR data. *Magnetic Resonance in Medicine*, 51(3), 586–594. <https://doi.org/10.1002/mrm.1072>
- Baselice, F., Ferraioli, G., Pascazio, V., & Sorriso, A. (2019). Denoising of MR images using Kolmogorov-Smirnov distance in a Non Local framework. *Magnetic Resonance Imaging*, 57, 176–193. <https://doi.org/10.1016/j.mri.2018.11.022>
- Maza-Quiroga, R., Thurnhofer-Hemsi, K., López-Rodríguez, D., & López-Rubio, E. (2021). Rician Noise Estimation for 3D Magnetic Resonance Images Based on Benford's Law. *Medical Image Computing and Computer Assisted Intervention – MICCAI 2021*, 340–349. [https://doi.org/10.1007/978-3-030-87231-1\\_33](https://doi.org/10.1007/978-3-030-87231-1_33)
- Chaudhari, A., & Kulkarni, J. (2021). Noise estimation in single coil MR images. *Biomedical Engineering Advances*, 2, 100017. <https://doi.org/10.1016/j.bea.2021.100017>
- Augustin, A. M., Kesavadas, C., & Sudeep, P. V. (2022). An Improved Deep Persistent Memory Network for Rician Noise Reduction in MR Images. *Biomedical Signal Processing and Control*, 77, 103736. <https://doi.org/10.1016/j.bspc.2022.103736>
- Karthick, S., & Jayasheela, M. FIREFLY OPTIMIZED PROBABILISTIC NEURAL NETWORK FOR BRAIN TUMOR CLASSIFICATION FROM MRI IMAGES.
- Dorjsembe, Z., Odonchimed, S., & Xiao, F. (2022, April). Three-Dimensional Medical Image Synthesis with Denoising Diffusion Probabilistic Models. In *Medical Imaging with Deep Learning*.
- Ding, Y., Yu, X., & Yang, Y. (2021). Modeling the Probabilistic Distribution of Unlabeled Data for One-shot Medical Image Segmentation. *Proceedings of the AAAI Conference on Artificial Intelligence*, 35(2), 1246–1254. <https://doi.org/10.1609/aaai.v35i2.16212>
- Sijbers, J., Poot, D., Dekker, A. J. den, & Pintjens, W. (2007). Automatic estimation of the noise variance from the histogram of a magnetic resonance image. *Physics in Medicine and Biology*, 52(5), 1335–1348. <https://doi.org/10.1088/0031-9155/52/5/009>
- Lili He, & Greenshields, I. R. (2009). A Nonlocal Maximum Likelihood Estimation Method for Rician Noise Reduction in MR Images. *IEEE Transactions on Medical Imaging*, 28(2), 165–172. <https://doi.org/10.1109/tmi.2008.927338>

- Rajan, J., den Dekker, A. J., & Sijbers, J. (2014). A new non-local maximum likelihood estimation method for Rician noise reduction in magnetic resonance images using the Kolmogorov–Smirnov test. *Signal Processing*, 103, 16–23. <https://doi.org/10.1016/j.sigpro.2013.12.018>
- Pizurica, A., Philips, W., Lemahieu, I., & Acheroy, M. (2003). A versatile wavelet domain noise filtration technique for medical imaging. *IEEE Transactions on Medical Imaging*, 22(3), 323–331. <https://doi.org/10.1109/tmi.2003.809588>
- Sahu, S., Singh, H. V., Kumar, B., & Singh, A. K. (2018). A Bayesian Multiresolution Approach for Noise Removal in Medical Magnetic Resonance Images. *Journal of Intelligent Systems*, 29(1), 189–201. <https://doi.org/10.1515/jisys-2017-0402>
- Rabbani, H., Nezafat, R., & Gazor, S. (2009). Wavelet-Domain Medical Image Denoising Using Bivariate Laplacian Mixture Model. *IEEE Transactions on Biomedical Engineering*, 56(12), 2826–2837. <https://doi.org/10.1109/tbme.2009.2028876>
- Hoffman, D., & Karst, O. J. (1975). The Theory of the Rayleigh Distribution and Some of Its Applications. *Journal of Ship Research*, 19(03), 172–191. <https://doi.org/10.5957/jsr.1975.19.3.172>

**APPENDICES****Appendix A****Ethical Approval Document**

There is no ethical approval document that can be presented.

Prof. Dr. Bülent BİLGEHAN

Supervisor

## Appendix B

### Curriculum Vitae

#### Personal Information

Surname, Name: MIRZAEI,Omid

Date of Birth: 19 Agust 1993

Place of Birth: Ahar, IRAN

Table B1.

#### *Education.*

Degree	Department/Program	University	Year of Graduation
B.Sc.	Biomedical Engineering	Near East University	2016
M.Sc.	Biomedical Engineering	Near East University	2019
P.hD	Biomedical Engineering	Near East University	Present

Table B2.

#### *Work Experience.*

Title	Place	Year
Officer	Near East University International Office	2013-2018
Biomedical Engineer	Dr. Suat Gonsel University of Kyrenia Hospital	2019
Biomedical Engineer	Cyprus Health and Social Sciences University	2019-2020
Research Assistan	Near East University Faculty of Engineering	2020-2021
Head of Department	Near East University Vacation School of Health Services, Department of Biomedical Device Technology	2021-Present
Research Assistant	NEU, Faculty of Engineering, Department of Computer Engineering	2014-2017
Lecturer	NEU, Faculty of Engineering, Department of Computer Engineering	2017-present

#### Foreign Languages

- Azerbaijani: Native language
- Persian: Country National language
- English: Fluent in reading, speaking, writing, listening

- Turkish: Full professional proficiency

### **Publications in International Journals and Conferences**

Gürman, M., Bilgehan, B., Sabuncu, Ö., & Mirzaei, O. (2022). A powerful probabilistic model for noise analysis in medical images. *International Journal of Imaging Systems and Technology*.

<https://doi.org/10.1002/ima.22838>

Aykac, A., Mirzaei, O., Tugce Cilingir Kaya, O., Ozbeyli, D., & Suer, K. (2022). Deep Learning-Based Histological Scoring of Cerulein-Induced Acute Pancreatitis Rat Model. *2022 International Conference on Artificial Intelligence in Everything (AIE)*.

<https://doi.org/10.1109/aie57029.2022.00022>

Bilgehan, B., & Mirzaei, O. (2021). Enhanced Hybrid Combiner Scheme for Wireless Network Communication. *2021 International Conference on Artificial Intelligence of Things (ICAIoT)*.

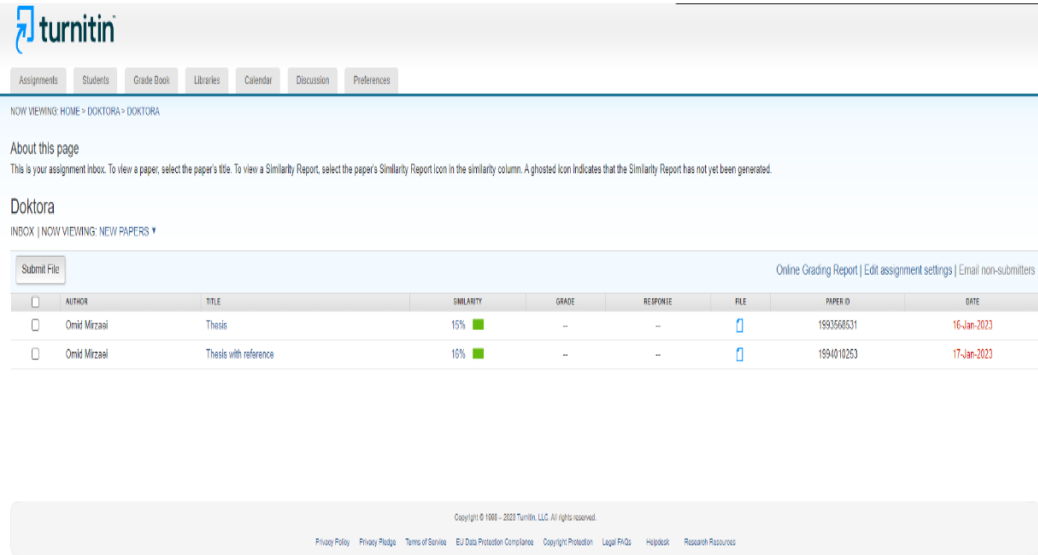
<https://doi.org/10.1109/icaiot53762.2021.00011>

Kibarar, G., Kaba, Ş., Mirzaei, O., & Köse, S. (2021). A Pioneer Approach for the Evaluation of Antihypertensive Drug Combinations Through Fuzzy PROMETHEE Method. *Advances in Intelligent Systems and Computing*, 760–765. [https://doi.org/10.1007/978-3-030-64058-3\\_95](https://doi.org/10.1007/978-3-030-64058-3_95)

Mirzaei, O., Aşıksoy, G., & Kibarar, A. G. (2021). Evaluation of the Management and Prevention of Covid-19 Pandemic in Most Infected Countries via Fuzzy PROMETHEE Approach. *Advances in Intelligent Systems and Computing*, 89–94. [https://doi.org/10.1007/978-3-030-64058-3\\_11](https://doi.org/10.1007/978-3-030-64058-3_11)

## Appendix C

### Similarity Report



turnitin

Assignments Students Grade Book Libraries Calendar Discussion Preferences

NOW VIEWING HOME > DOKTORA > DOKTORA

About this page  
This is your assignment inbox. To view a paper, select the paper's title. To view a Similarity Report, select the paper's Similarity Report icon in the similarity column. A ghosted icon indicates that the Similarity Report has not yet been generated.

Doktora  
INBOX | NOW VIEWING: NEW PAPERS ▾

Submit File Online Grading Report | Edit assignment settings | Email non-submitters

<input type="checkbox"/>	AUTHOR	TITLE	SIMILARITY	GRADE	RESPONSE	FILE	PAPER ID	DATE
<input type="checkbox"/>	Omid Mirzaei	Thesis	15% <span style="color: green;">■</span>	--	--		1993568531	16-Jan-2023
<input type="checkbox"/>	Omid Mirzaei	Thesis with reference	16% <span style="color: green;">■</span>	--	--		1994010253	17-Jan-2023

Copyright © 1998 - 2023 Turnitin, LLC. All rights reserved.

Privacy Policy Privacy Notice Terms of Service EU Data Protection Compliance Copyright Protection Legal FAQs Helpdesk Research Resources

Prof. Dr. Bülent BİLGEHAN

Supervisor